Inorganic Chemistry

pubs.acs.org/IC Article

# Silica Nanopowder Supported Frustrated Lewis Pairs for $CO_2$ Capture and Conversion to Formic Acid

Kgauhelo Mentoor, Linette Twigge, J. W. Hans Niemantsverdriet, Jannie C. Swarts, and Elizabeth Erasmus*

Cite This: *Inorg. Chem.* 2021, 60, 55−69 Read Online

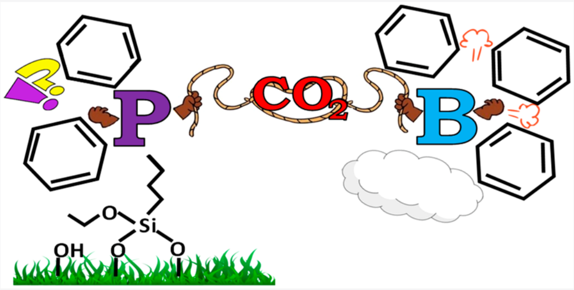

**ABSTRACT:** Treatment of hydroxylated silica nanopowders **S1** and allyl-functionalized silica nanopowders **S2** with 3-(diphenylborano)- or 3-bis(pentafluorophenylborano)propyltrimethoxysilane or 2-(diphenylphosphino)- or 2-(dicyclohexylphosphino)ethyltriethoxysilane generates silica nanopowder supported Lewis acids **S3** and silica nanopowder supported Lewis bases **S4**. These surfaces were characterized by $^{13}C$, $^{11}B$, and $^{31}P$ cross-polarization magic angle spinning nuclear magnetic resonance (CP MAS NMR), X-ray photoelectron spectroscopy (XPS), and attenuated total reflection Fourier transform infrared (ATR FTIR). When **S3** is combined with solution-phase Lewis bases $PR_3$ (R = $C_6F_5$, $C_6H_5$, mesityl), six associated silica nanopowder supported frustrated Lewis pairs (FLPs) are formed. In another set of six reactions, the interactions between the supported Lewis bases **S4** and solution-phase Lewis acids $BR_3$ with R = $C_6F_5$, $C_6H_5$, mesityl produced six more associated supported FLPs. The capture of $CO_2$ by these FLPs producing FLP-$CO_2$ Lewis pair adducts **S5** and **S6** were highlighted by ATR FTIR, and it was found that FLP **S5e** with R = $C_6H_5$ on both the supported Lewis acid and solution-phase Lewis base trapped the largest quantities of $CO_2$ on the silica nanopowder supports. Conversion of $CO_2$ to HCOOH was achieved by first activating $H_2$ to generate activated FLP-$H_2$ surfaces **S7** and **S9**. Addition of $CO_2$ then generated HCOOH via the silica nanopowder supported FLP-HCOOH adducts **S8** and **S10**. Qualitative identification of HCOOH generation was achieved by ATR FTIR measurements, and surface **10b** with R = $C_6H_5$ proved to be the most successful silica nanopowder surface bound FLP in HCOOH generation. In some cases, diborano formates (−BO(CH)OB−) **S11** and **S12** were also identified as side products during HCOOH formation. Spectroscopic characterization of purposefully synthesized **S11** and **S12** included $^{11}B$ and $^{31}P$ CP MAS NMR.

## ■ INTRODUCTION

Carbon sequestration is a procedure where $CO_2$ is captured and stored to limit the influence of $CO_2$ on climate change. An alternative to merely storing the $CO_2$ is to convert the captured $CO_2$ into industrially important chemicals such as formaldehyde, formic acid, and methanol. This can be achieved by the reduction of $CO_2$ with $H_2$. Due to the chemical inertness and thermodynamic stability of $CO_2$, harsh conditions are normally required for this reduction. For the reduction of $CO_2$ to proceed under milder conditions, organometallic catalysts may be used.[1,2] However, with the discovery and development of frustrated Lewis pairs (FLPs),[3,4] the metal-free capture, activation, and subsequent catalytic conversion of small molecules such as $CO_2$ and $NO_2$ to industrially important feedstock chemicals is possible.[5−8] Combinations of a bulky Lewis acid and a bulky Lewis base which are so sterically hindered that they prohibit the formation of normal Lewis adducts produce these FLPs. An example of an FLP would be the combination of triphenylphosphine, $P(C_6H_5)_3$, a bulky Lewis base, and the borane $B(C_6F_5)_3$, a bulky Lewis acid.

Despite all the successes obtained by FLPs in solution, hardly any attempts have been made to anchor these FLPs onto a solid support to create a heterogeneous catalytic system.[9−14] The first catalytic report of a solid-phase FLP system showed that the combination of a gold surface with a Lewis base (either imines or nitriles) could activate hydrogen and cause hydrogenation of unsaturated compounds.[15] While some semi-immobilized FLP systems have been prepared by impregnation of $B(C_6F_5)_3$ in either a triarylphosphine polymer or a polyamine organic framework, $H_2$ activation[16] and hydrogenation of the electron-poor alkene diethyl benzylidenemalonate were possible.[17] Additionally, $B(C_6F_5)_3$ has also been used in combination with cyclodextrin or molecular sieves for a number of different reactions, including hydrogenation and reductive deoxygenation

**Received:** July 8, 2020
**Published:** December 22, 2020

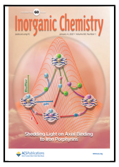

https://dx.doi.org/10.1021/acs.inorgchem.0c02012
*Inorg. Chem.* 2021, 60, 55−69

Scheme 1. Syntheses of Boranes 1, Supported Lewis Acids S3, and Supported Lewis Bases S4

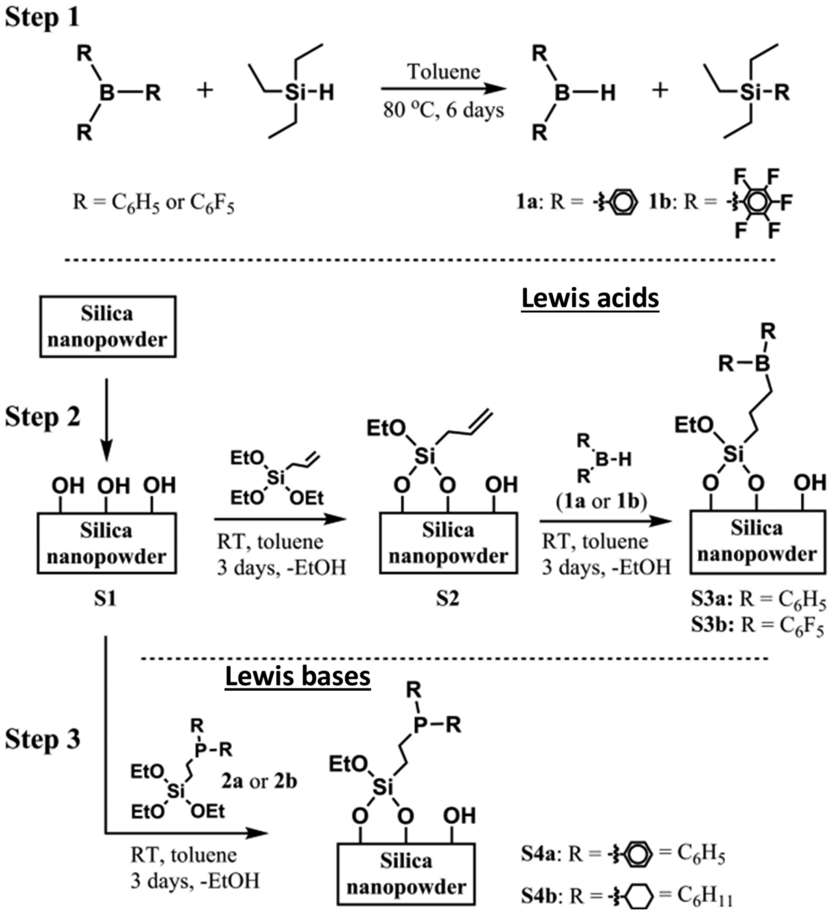

of ketones.[18] Only a few reports of silica-supported Lewis acids where the Lewis base FLP partners are still in the solution phase are available.[19,20] Szeto and co-workers[21] showed an FLP derived from a phosphine Lewis base supported on an aluminum infused silica and Piers' reagent, $HB(C_6F_5)_2$, as the Lewis acid partner were active in the catalytic hydrogenation of alkynes. In addition, amines and phosphines were introduced on Ti-, Al-, and Zr-metalated SBA-15 surfaces and tested for $CO_2$ adsorption.[22]

The advantage of heterogeneous over homogeneous catalysts is the ease of separation from the product, the recyclability of the catalyst, and the prospect of using a continuous flow reactor on an industrial scale.

In this study, we demonstrate the direct grafting of triethoxysilane-functionalized Lewis acids and bases onto hydroxylated silica nanopowder as a new approach to preparing supported (heterogeneous) Lewis acids and bases. The interaction between the heterogeneous solid silica-supported Lewis acid (or silica-supported Lewis base) and a dissolved Lewis base (or dissolved Lewis acid) as the frustrated Lewis pair partner produces associated heterogeneously supported FLPs. The ability of these silica nanopowder supported FLPs to capture, release, and convert $CO_2$ to formic acid, HCOOH, is also demonstrated.

## ■ EXPERIMENTAL SECTION

**Materials and General Procedures.** 2-(Diphenylphosphino)-ethyltriethoxysilane and dicyclohexylphosphinoethyltriethoxysilane were purchased from ABCR GmbH and used without further purification. The following solid reagents were purchased from Sigma-Aldrich and were purified by sublimation: triphenylphosphine, tris(2,4,6-trimethylphenyl)phosphine, tris-(pentafluorophenylphosphine), triphenylborane, trimesitylborane, tris-(pentafluorophenyl)borane, triethylsilane, and allyltriethoxysilane. Silicon dioxide nanopowder (spherical, porous, 5−15 nm particle size (TEM), 99.5%, Sigma-Aldrich) was used as is without further purification. Deuterated benzene and chloroform were obtained from Cambridge Isotope Laboratories, Inc., and solvents from Merck Chemicals. Toluene, hexanes, and THF were dried and purified by distilling over sodium. Filtration and vacuum evaporation were conducted with the help of a vacuum pump to avoid moisture. Unless otherwise stated, all handling and storage of chemicals and solvents were conducted in an MBraun Labmaster Sp glovebox under a nitrogen atmosphere having water and oxygen levels below 12 ppm.

**Spectroscopic Characterization Techniques.** *X-ray Photoelectron Spectroscopy.* XPS was conducted on a PHI 5000 Versaprobe spectrometer using monochromatic Al K$\alpha$ radiation ($h\nu$ = 1253.6 eV), to characterize the surfaces of the modified silica nanopowders. The specific details of the XPS study are similar to those of other XPS studies reported from our laboratory.[23−29]

*Nuclear Magnetic Resonance.* Solution-phase $^1H$ NMR measurements were recorded on a Bruker Fourier 300 MHz spectrometer operating at 300.13 MHz. Chemical shifts are reported relative to $SiMe_4$ at 0.00 ppm.

Solid-state NMR spectra were collected on a 400 MHz Bruker Avance III spectrometer equipped with a 4 mm VTN multinuclear double-resonance magic angle spinning probe, operating at 25 °C. All solid-state samples were packed in 4 mm zirconia rotors and were spun at 14000 Hz during measurements for all the different nuclei; protons were decoupled. The $^{13}C$ NMR spectra were recorded at 100.6 MHz, using the cross-polarization magic angle spinning (CP MAS) technique.

**Scheme 2. $CO_2$ Capture by Supported Lewis Acid (S3) and Dissolved Lewis Base (3) mixtures (Left) or by Supported Lewis Base (S4) and Dissolved Lewis Acid (4) Mixtures (Right) to Give the FLP/$CO_2$ Adducts S5 and S6, Respectively**

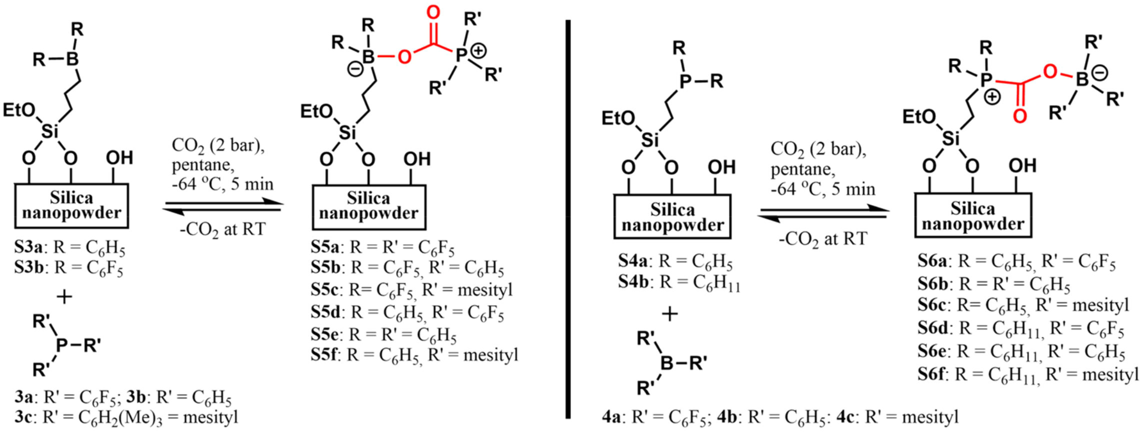

The contact time was 2 ms. A recycle delay of 5 s and an acquisition time of 33.9 ms were used. $^{13}C$ resonances are referenced vs adamantane as an external standard.

The $^{11}B$ NMR spectra were recorded at 128.4 MHz, with a contact time of 5 ms, a recycle delay of 2 s, and an acquisition time of 49.9 ms. The $^{31}P$ NMR spectra were recorded at 162.0 MHz, with a contact time of 5 ms, a recycle delay of 2 s, and an acquisition time of 49.9 ms. The $^{11}B$ CP MAS NMR spectra are referenced vs $NaBH_4$ as an external standard, and the $^{31}P$ CP MAS NMR spectra are referenced vs $H_3PO_4$ as an external standard.

*Attenuated Total Reflectance Fourier Transform Infrared Spectroscopy.* ATR FTIR spectra of samples in the solid or liquid phase were recorded as neat samples on a Nicolet IS50 FTIR spectrometer equipped with a single-bounce ATR diamond.

**Syntheses.** Scheme 1 illustrates the syntheses of **1** and **S1**−**S4**.

*Diphenylborane (**1a**) and Bis(pentafluorophenyl)borane (**1b**).* In a glovebox, either triphenylborane (0.504 g, 2.082 mmol) or tris(pentafluorophenyl)borane (1.001 g, 1.95 mmol) were transferred to a flask containing 10 mL of dry $O_2$-free toluene. The two separate mixtures were stirred until the boranes were fully dissolved. This was followed by the slow dropwise addition of a 10 mL oxygen-free toluene solution of triethylsilane (0.243 g, 0.33 mL, 2.097 mmol) to the $B(C_6H_5)_3$ solution or of triethylsilane (0.230 g, 0.31 mL, 1.980 mmol) to the $B(C_6F_5)_3$ solution. The mixtures were heated to 80 °C and stirred at this temperature for 6 days. As **1a** and **1b** formed, the solutions turned yellow and brown, respectively. The solutions were then cooled to room temperature and subsequently concentrated to ca. 15 mL. This caused immediate precipitation of the desired products. Solid **1a** and **1b** were isolated by filtration and washed three times with dry, $O_2$-free toluene to remove residual $Et_3SiH$.

Solid $(C_6H_5)_2BH$ (**1a**) was obtained as a fluffy, fibrous white powder (0.067 g, 27.7%), mp 214.3 °C, and was stored in a glovebox. ATR FTIR/$cm^{-1}$: $\nu$(B−H) 1574. $^1H$ NMR $\delta_H$ (300 MHz, $C_6D_6$)/ppm: 4.02 (1 × 1H, s, B−H), 7.35−7.38 (6H, m, 2 × $C_6H_5$), 8.25−8.27 (4H, m, 2 × $C_6H_5$).

Solid $(C_6F_5)_2BH$ (**1b**) was obtained as a white crystalline powder (0.12 g, 17.8%), mp 114.0 °C, and was stored in a glovebox. ATR FTIR/$cm^{-1}$: $\nu$(B−H) 1564 (characteristic of a B−($\mu$-H)$_2$−B function).[30] $^1H$ NMR $\delta_H$ (300 MHz, $C_6D_6$)/ppm: 4.18 (1 × 1H, s, B−H) (see the Supporting Information for ATR FTIR and NMR spectra, respectively).

*Silica Nanopowder Supported Allyltriethoxysilane (**S2**).* Silica nanopowder was boiled for 1 h in double-distilled water to generate surface **S1** (Scheme 1, step 2) bearing hydroxyl groups and then dried for 16 h under vacuum ($10^{-3}$ mm Hg) at 60 °C. Allyltriethoxysilane (1 g, 4.89 mmol) was then added to a slurry of the hydroxylated silica nanopowder (**S1**, 0.28g) in dry $O_2$-free toluene (10 mL). The resulting mixture was stirred at room temperature in a glovebox for 3 days. The mixture was then filtered, and the recovered white powder waswashed with dry $O_2$-free toluene (3×) before the residual solvent was allowed to evaporate in the glovebox over 2 days. Final solvent removal was by vacuum evaporation ($P < 10^{-3}$ mmHg) to afford 0.303 g of silica nanopowder supported allyltriethoxysilane **S2** as a white powder. ATR FTIR/$cm^{-1}$: $\nu$(C=C) 1633, $\nu$(C−H) 2898−3084. $^{13}C$ CP MAS NMR $\delta_C$ (100.6 MHz)/ppm: 21.23 (C5), 23.02 (C3), 62.74 (C4), 119.07 (C1), 135.52 (C2).

*Silica Nanopowder Supported Diphenylborane (**S3a**) and Bis(pentafluorophenyl)borane (**S3b**).* The boranes **1a** (0.026 g, 0.156 mmol) and **1b** (0.014 g, 0.040 mmol) were added to slurries of **S2** (0.199 g for **1a** or 0.123 g for **1b**) in dry $O_2$-free toluene (10 mL) (Scheme 1, step 2). The resulting mixtures were stirred at room temperature in a glovebox for 3 days. The mixtures were then filtered, the resulting white powders were washed with dry $O_2$-free toluene (3×), and residual solvent was allowed to evaporate in the glovebox over 2 days. Further solvent removal was carried out by vacuum evaporation ($P < 0.001$ mmHg) to afford either **S3a** (0.157 g) or **S3b** (0.036 g) as a white powder.

Data for **S3a** are as follows. ATR FTIR/$cm^{-1}$: $\nu$(B−phenyl) = 1440, $\nu$(C−H) 2872−3076. $^{13}C$ CP MAS NMR $\delta_C$ (100.6 MHz)/ppm: 19.82 (C2), 21.78 (C5), 22.94 (C3), 40.76 (C1), 62.55 (C4), 130.67 (C8,8′; C9,9′; C10,10′), 134.25 (C7,7′; C11,11′), 138.52 (C6,6′). $^{11}B$ CP MAS NMR $\delta_B$ (128.4 MHz)/ppm: −0.31.

Data for **S3b** are as follows. ATR FTIR/$cm^{-1}$: $\nu$(B−Phenyl) 1486, $\nu$(C−H) 2894−3011. $^{13}C$ CP MAS NMR $\delta_C$ (100.6 MHz)/ppm: 17.68 (C2), 19.34 (C5), 22.46 (C3), 33.10 (C1), 62.34 (C4), 128.89 (C6,6′), 131.86 (C8,8′; C9,9′; C10,10′), 132.44 (C7,7′; C11,11′). $^{11}B$ CP MAS NMR $\delta_B$ (128.4 MHz): −0.44.

*Silica Nanopowder Supported 2-(Diphenylphosphino)ethyltriethoxysilane (**S4a**) and 2-(Dicyclohexylphosphino)ethyltriethoxysilane (**S4b**).* The phosphine silanes, either 2-(diphenylphosphino)ethyltriethoxysilane **2a** (1.01 g, 2.68 mmol for **S4a**) or 2-dicyclohexylphosphinoethyltriethoxysilane **2b** (1.011 g, 2.60 mmol for **S4b**) were added to a slurry of hydroxy-covered silica nanopowder **S1** (see synthesis of **S2** for how to obtain **S1**; 0.152 g for **S4a** or 0.145g for **S4b**) in dry $O_2$-free toluene (10 mL) (Scheme 1, step 3). The resulting solutions were stirred at room temperature in a glovebox for 3 days. The solutions were then filtered, the recovered white powder was washed with dry $O_2$-free toluene (3×), and the adsorbed solvent on the powder was allowed to evaporate in a glovebox over 2 days. Final solvent removal was carried out by vacuum evaporation to afford either **S4a** (0.118 g) or **S4b** (0.107 g) as a white powder.

Data for **S4a** are as follows. ATR FTIR/$cm^{-1}$: $\nu$(P−C) 1447, $\nu$(C−H) 2855−2969. $^{13}C$ CP MAS NMR $\delta_C$ (100.6 MHz)/ppm: 9.97 (C2), 21.45 (C1), 24.28 (C4), 62.33 (C3), 131.86 (C7,7′; C8,8′; C9,C9′), 136.16 (C6,6′; C10,10′), 138.43 (C5,5′). $^{31}P$ CP MAS NMR $\delta_P$ (162.0 MHz)/ppm: $\delta$ −5.56.

Data for **S4b** are as follows. ATR FTIR/$cm^{-1}$: $\nu$(C−H) 2883−3054 $cm^{-1}$. $^{13}C$ CP MAS NMR $\delta_C$ (100.6 MHz)/ppm: 6.52 (C2), 10.16

**Table 1. Supported Lewis Acid/Base S3 or S4 Used in Combination with Dissolved Lewis Base/Acid 3 or 4 to Trap $CO_2$**[a]

| supported Lewis acid | mass/g **S2** used | dissolved Lewis base (mass/mg) | product | supported Lewis base | mass/g of **S4** used | dissolved Lewis acid (mass/mg) | product |
|---|---|---|---|---|---|---|---|
| **S3a**, R = $C_6H_5$ | 0.020 | **3a**: $P(C_6F_5)_3$ (20) | **S5a** | **S4a**, R = $C_6H_5$ | 0.040 | **4a**: $B(C_6F_5)_3$ (7) | **S6a** |
| | 0.026 | **3b**: $P(C_6H_5)_3$ (10) | **S5b** | | 0.041 | **4b**: $B(C_6H_5)_3$ (4) | **S6b** |
| | 0.020 | **3c**: $P(Mes)_3$, (15) | **S5c** | | 0.040 | **4c**: $B(Mes)_3$ (5) | **S6c** |
| **S3b**, R = $C_6F_5$ | 0.020 | **3a**: $P(C_6F_5)_3$ (29) | **S5d** | **S4b**, R = $C_6H_{11}$ | 0.029 | **4a**: $B(C_6F_5)_3$ (5) | **S6d** |
| | 0.029 | **3b**: $P(C_6H_5)_3$ (15) | **S5e** | | 0.030 | **4b**: $B(C_6H_5)_3$ (3) | **S6e** |
| | 0.020 | **3c**: $P(Mes)_3$ (21) | **S 5f** | | 0.030 | **4c**: $B(Mes)_3$ (4) | **S6f** |

[a] Mes = 2,4,6-trimethylphenyl.

(C2), 20.33 (C8,C8′), 21.79 (C7,C7′; C9,9′), 24.42 (C6,6′; C10,10′), 30.07 (C5,5′), 61.69 (C3). $^{31}P$ CP MAS NMR $\delta_P$ (162.0 MHz)/ppm: 5.60.

**$CO_2$ Capture.** Reactions were as shown in Scheme 2.

*Utilizing Silica Nanopowder Supported Lewis Acids **S3**.* A two-neck round-bottom flask was flame-dried under vacuum and filled with $CO_2$ until atmospheric pressure (3×). **S3** was then suspended in argon-degassed pentane (5 mL) in the two-neck round-bottom flask (details in Table 1), and $CO_2$ was bubbled through this suspension. This was followed by the addition of Lewis bases **3** (Table 1). The reaction flask was cooled to −64 °C with a chloroform/dry ice slurry and pressurized with $CO_2$ until 2.0 bar, and the contents were stirred for 5 min. The precipitated white solid of **S5** was isolated from the pentane solution by removing the solvent with a vacuum pump ($10^{-3}$ mm Hg) at −64 °C and analyzed by ATR FTIR at both low (−64 °C) and room temperature.

*Utilizing Silica Nanopowder Supported Lewis Bases **S4**.* The experimental procedure was as described for the supported Lewis acids **S3** above, but utilizing the supported Lewis bases **S4** and dissolved Lewis acids **4** as FLP partners. Quantities used are given in Table 1.

**$CO_2$ Conversions by Supported FLPs.** Scheme 3 highlights the reaction sequences.

*$H_2$ Activation to Give **S7** or **S9**.* **S3** (0.02 g) or **S4** (0.04 g) was added to oxygen-free pentane (10 mL) in a previously flame-dried and Ar-filled two-neck, round-bottom flask to afford a slurry. This was followed by the addition of either **3** (3−5 mg to **S3**) or **4** (3−7 mg to **S4**) in the flask equipped with two taps. The reaction flask was then evacuated and refilled with $H_2$ (2.0 bar; *Caution*! no open flames or any other ignition source) and stirred at room temperature for 3 days. Pentane and any other volatiles were then removed from the white precipitate **S7** or **S9** with a vacuum pump ($10^{-3}$ mmHg).

*$CO_2$ Conversion.* After $H_2$ activation to obtain **S7** or **S9**, the H-activated FLP system was immediately added to toluene (10 mL) in a previously flame-dried and Ar-filled (3×) two-neck, round-bottom flask equipped with two taps. The pressure in the reaction flask was lowered to ca. $10^{-3}$ mmHg to remove the Ar atmosphere, after which it was pressurized with $CO_2$ to 2.0 bar and the contents were stirred for 3 days at 60 °C. The resulting yellow precipitate consisting of **S13** or **S14** was isolated from the toluene solution by removing the solvent at reduced pressure ($10^{-3}$ mmHg, vacuum pump), rinsing with DCM (2×), and filtered using a filter paper. The precipitate was analyzed by ATR FTIR. **S13** and **S14** form via **S8** and **S10**. For **S8a** and **S8d**, not only **S13** formed. The precipitated product also contained by virtue of ATR FTIR and $^{11}B$ and $^{31}P$ CP MAS experiments traces of side products consistent with the diborano formate species **S11a** and **S11d** (Scheme 3, top). Similarly, intermediates **S10b**, **S10d**, and **S10e** (Scheme 3 bottom mechanism) did not only rearrange to give formic acid. **S14** was partially contaminated with **S12b**, **S12d**, or **S12e**.

*Direct Preparation of **S11a** and **S11d**.* To confirm the formation of **S11a** and **S11d**, surface **S3a** or **S3b** (0.02 g) was suspended in toluene (5 mL). To this was added **3a** (4 mg) dissolved in toluene (5 mL). A ca. 50-fold excess of formic acid (0.15 mL) was then added to the FLP system and the resultant mixture was stirred at 60 °C for 1 h. All liquids (volatiles) were removed under vacuum, and the residue was analyzed by ATR FTIR and solid-state NMR ($^{13}C$, $^{1}B$, and $^{31}P$) to identify the diborano esters of **S11a** and **S11d**. Similar experiments utilizing **S3a** or **S3b** together with **3b** or **3c** and formic acid failed to generate the diborano ester surfaces **S11b**, **S11c**, **S11e**, and **S11f** in quantities that could be detected by ATR FTIR and solid-state $^{13}C$, $^{1}B$, and $^{31}P$ NMR. Data for **S11d**: IR/cm$^{-1}$: $\nu(C\underline{..}O)$ 1640. Data for **S11a**: ATR FTIR/cm$^{-1}$:$\nu$ $(C\underline{..}O)$ 1638. $^{13}C$ CP MAS NMR $\delta_C$ (100.6 MHz)/ppm: 5.4; 25.9; 115.1; 132.9; 167.6. $^{11}B$ CP MAS NMR $\delta_B$ (128.4 MHz)/ppm: 0.07; 12.4. $^{31}P$ CP MAS NMR $\delta_P$ (162.0 MHz)/ppm: 35.9; 62.1.

*Direct Preparation of **S12b,d,e**.* Surface **S4a** or **S4b** (40 mg) was suspended in toluene (5 mL). To each of these suspensions was added **4a**, **4b**, or **4c** dissolved in toluene (5 mL). A ca. 50-fold excess of formic acid (0.15 mL) was then added to the FLP system, and the resultant mixture was stirred at 60 °C for 1 h. All volatiles were removed under vacuum, and the liquid-free residue was analyzed by ATR FTIR and solid-state NMR ($^{13}C$, $^{11}B$, and $^{31}P$). Diborano formate surfaces **S12b** (obtained from **S4a** and **4b**), **S12d** (from **S4b** and **4a**), and **S12e** (from **S4b** and **4b**) (Scheme 3, bottom) were identified. Similar experiments utilizing formic acid, **S4a**, and either **4a** (to generate **12a**) or **4c** (to generate **12c**) or formic acid, **S4b**, **4c** to generate **S12f** failed to generate the expected diborano formate surfaces **S12a**, **S12c**, and **S12f** in quantities that could be detected by ATR FTIR and solid-state $^{13}C$, $^{11}B$, and $^{31}P$ NMR. Data for **S12b**: IR (cm$^{-1}$): $\nu(C\underline{..}O)$ 1639. Data for **S12d**: IR (cm$^{-1}$): $\nu(C\underline{..}O)$ 1640. Data for **S12e**: IR (cm$^{-1}$): $\nu(C\underline{..}O)$ 1640. $^{13}C$ NMR $\delta_C$ (100.6 MHz)/ppm: 5.7; 26.3; 112.6; 132.5; 168.2. $^{11}B$ CP MAS NMR $\delta_B$ (128.4 MHz): −0.2; 13.3 ppm. $^{31}P$ CP MAS NMR $\delta_P$ (162.0 MHz): 33.4; 59.2 ppm.

## ■ RESULTS AND DISCUSSION

**Syntheses.** The multistep reaction sequences followed during the preparation of the supported Lewis acids (boranes) and supported Lewis bases (phosphines) are illustrated in Scheme 1. Commercially available triphenylborane or tris(pentafluorophenyl)borane was first reacted (step 1) with an excess of triethylsilane to afford either diphenylborane (**1a**) or bis(pentafluorophenyl)borane (**1b**). During this reaction one $-C_6H_5$ or $-C_6F_5$ group of each of the boranes is exchanged with the proton of triethylsilane.

Step 2 of Scheme 1 highlights the anchoring of the Lewis acids on modified silica nanopowder supports. The silica nanopowder is first hydroxylated in boiling water to generate **S1**. Allyltriethoxysilane is then grafted onto the hydroxylated nanosilica **S1** to produce the allyl-capped surface **S2**. The double bond on the silane provides a covalent anchoring site for borane-based Lewis acids **1a** and **1b**. In the ensuing hydroboration reactions, the Lewis acid boranes **1a** and **1b** react with the allyl groups of the surface of **S2**. Hydrogen atom transfer to the $\beta$-carbon of the allyl group takes place, while the boron attaches to the terminal $\gamma$-carbon relative to the Si atom of **S2**. This results in the formation of silica-supported Lewis acids **S3a** and **S3b**.

The preparation of the supported Lewis bases **S4a** and **S4b** required fewer reaction steps (Scheme 1, step 3). Commercially available 2-(diphenylphosphino)ethyltriethoxysilane (**2a**) and 2-(dicyclohexylphosphino)ethyltriethoxysilane (**2b**) were both

**Scheme 3. Reaction A, $H_2$ Activation by the Supported Lewis Acid S3 (top) or Lewis Bases S4 (Bottom) and FLP Partners 3 and 4 to Give $[-B^{\ominus}H][HP^{\oplus}-]$ Salts S7 and S9,[a,b] and Reaction B, Purposeful Preparation of S11 and S12, as Shown on the Right Half of the Scheme**

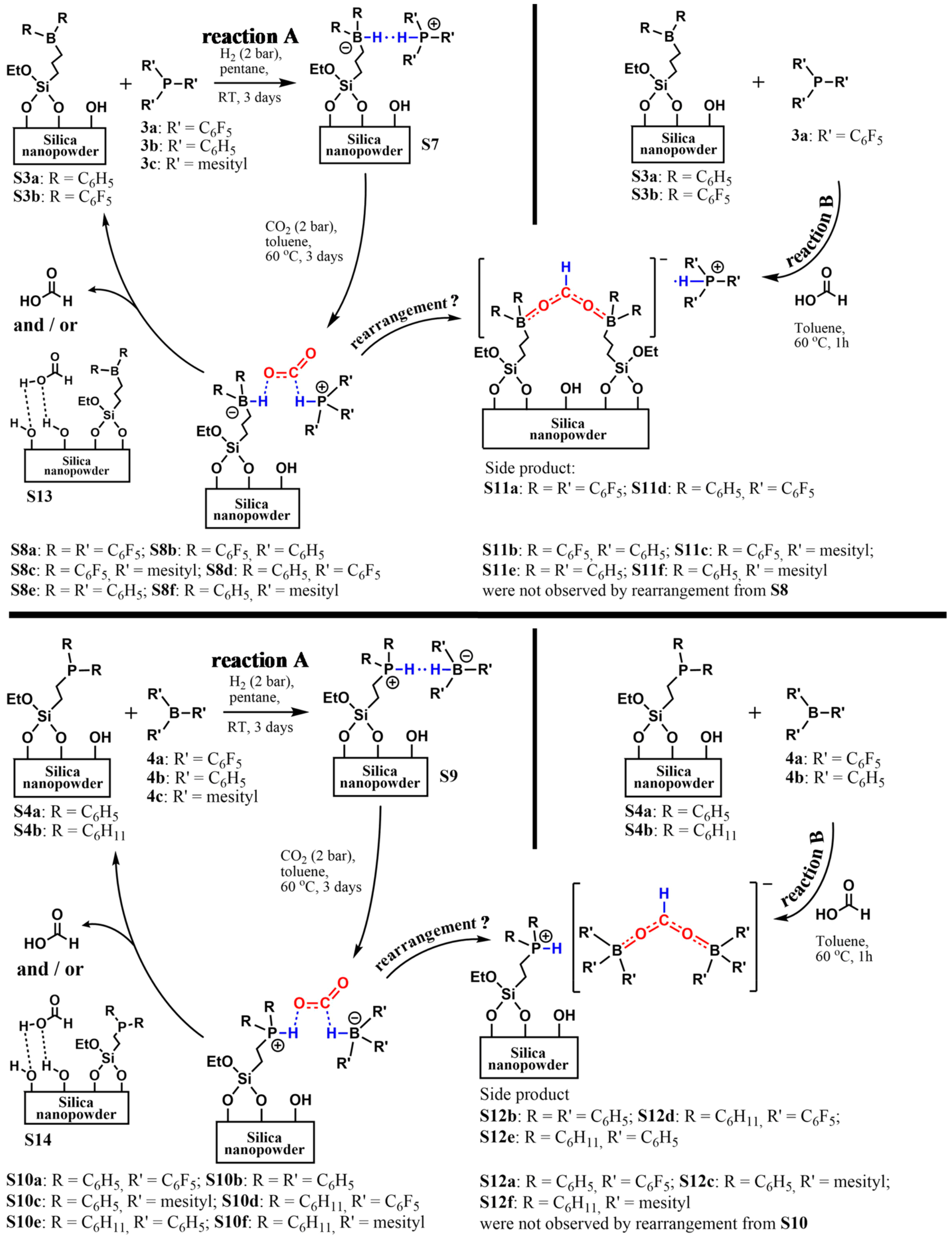

[a] **S7** and **S9** have components **a**–**f**, R and R′ combinations are as defined for **S8** and **S10**, respectively. Addition of $CO_2$ ultimately leads after hydrogenation via intermediate **S8** or **S10** to free and/or adsorbed HCOOH (**S13** or **S14**). [b] Free HCOOH might be released, or it may absorb on support **S13** or **S14** after it dissociated from **S8** or **S10**. Analyses were on **S8** and **S10** (which converted to **S13** and **S14**), but the small reaction scale and reduced-pressure workup prevented free HCOOH detection. Diborano formate side products **S11** and **S12** formed by rearrangement of **S8** or **S10** and/or by reaction of FLP precursors **S3** and **3** (or **S4** and **4**) with the newly formed HCOOH (similar to reaction B).

anchored in two separate reactions onto the hydroxylated nanosilica surface **S1** to produce **S4a** and **S4b**, respectively.

Subsequent introduction of stoichiometric amounts of either soluble $PR_3$ (R = $C_6F_5$, $C_6H_5$, mesityl) or soluble $BR_3$ (R = $C_6F_5$, $C_6H_5$, mesityl) to insoluble **S3** or **S4**, respectively, results in the formation of associated silica nanopowder supported frustrated Lewis pairs (FLPs). These reactions are shown inScheme 2 and discussed in the text associated with it.

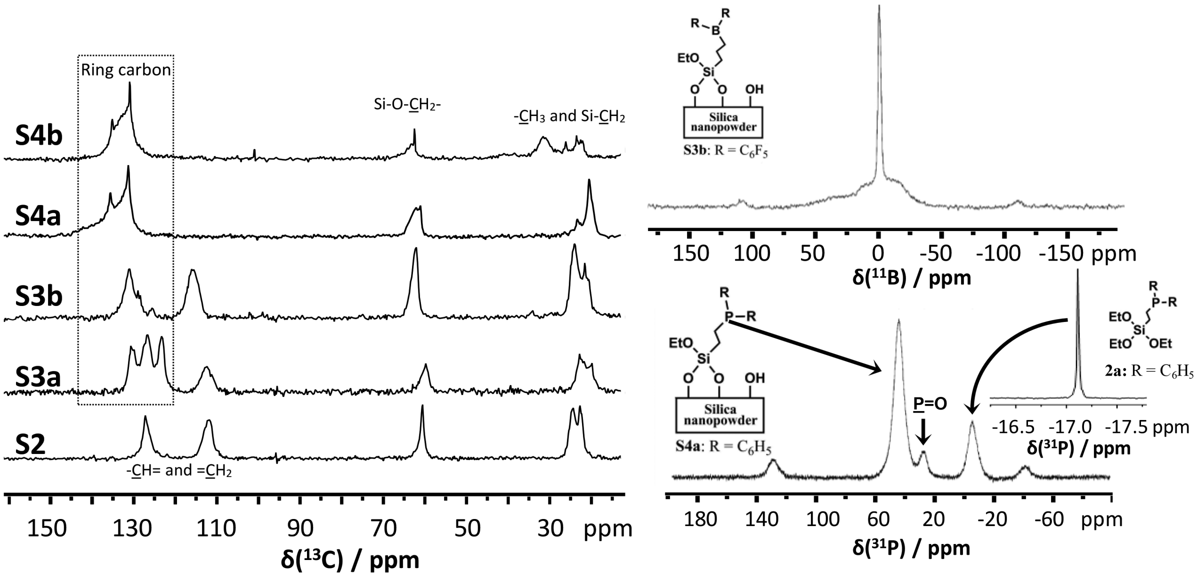

**Figure 1.** (left) $^{13}$C solid-state NMR of the silica nanopowder supported allyltriethoxysilane (**S2**), 3-(diphenylborano)- (**S3a**) and 3-(bis(pentafluorophenylborano))propyltriethoxysilane (**S3b**), and 2-(diphenylphosphino)- (**S4a**) and bis(cyclohexylphosphino)ethyltriethoxysilane (**S4b**). Functional groups responsible for resonances are shown on the spectra. (top right) $^{11}$B CP MAS NMR of **S3b.** (bottom right) $^{31}$P CP MAS NMR of **S4a**. (insert bottom right) $^{31}$P solution-phase NMR of the reactant **2a** required to prepare surface **S4a**.

**Spectroscopic Characterization.** To confirm the formation of the correct surfaces **S2**−**S4**, solid-state $^{13}$C, $^{11}$B, and $^{31}$P NMR, ATR FTIR, and X-ray photoelectron spectroscopy (XPS) experiments were performed.

*$^{13}$C, $^{11}$B, and $^{31}$P Solid-State NMR.* Figure 1 (left) shows the $^{13}$C solid-state NMR spectra of **S2**−**S4**. The resonances at 15−30 ppm are assigned to the $CH_3$ groups of the ethoxys bound to Si, $SiOCH_2CH_3$, and the $CH_2$ carbon $\alpha$ to the Si, i.e. $SiCH_2$, of **S2** and **S3**. The presence of the $SiOCH_2$ ethoxy carbon is evidenced by the resonances at a chemical shift of 55−65 ppm, while that of the vinylic carbons of **S2** is located between 110 and 130 ppm. The resonances between 120 and 145 ppm are assigned to the aromatic ring carbons. The presence of the $SiOCH_2$ CP MAS $^{13}$C NMR resonances of the ethoxy moiety at 55−65 ppm of all surfaces implies that at least one of the ethoxy moieties of the silanes has reacted with the hydroxylated surface, but not all three. In the CP MAS $^{13}$C NMR spectra of **S3**, the presence of vinylic carbon resonance signals implies that complete hydroboration of the double bonds did not occur.

The mere fact that some vinylic protons were still detected in **S3** and that not all the ethoxy moieties in **S3** were replaced during silane binding to **S2** meant that there is a possibility that some of boranes **1** added to **S2** (Scheme 1) might have bonded to free OH groups in an uncatalyzed dehydrocoupling reaction. To eliminate the possibility that uncatalyzed dehydrocoupling of $R_2BH$ **1a** or **1b** to **S2** occurred to generate $\equiv SiOB(C_6F_5)_2$ or $\equiv SiOB(C_6H_5)_2$ pollution on **S3** surfaces, $^{11}$B CP MAS NMR spectra of **S3** were measured. Figure 1 (top right) shows the spectrum for surface **S3b** ($R = C_6F_5$); the spectrum for **S3a** ($R = C_6H_5$) may be found in Figure S4 in the Supporting Information. The $^{11}$B CP MAS NMR spectra of **S3a** and **S3b** exhibit a single resonance at −0.31 and −0.44 ppm, respectively. The replacement of the fluorine atoms (5 per phenyl ring, thus 10 in all) with protons only causes a 0.13 ppm upfield shift. This small upfield shift is mirrored by the relatively small reported[31] upfield shift of ca. 1.5 ppm in the $^{11}$B NMR spectra for $B(OC_6H_5)_3$ at 16.5 ppm and $B(OC_6F_5)_3$ at 15.0 ppm. Since there is only one peak present in the $^{11}$B CP MAS NMR of **S3**, it implies that a single type of borane species is present on the surface. To eliminate the possibility that the $^{11}$B CP MAS NMR resonances of **S3a** and **S3b** at −0.31 and −0.44 ppm are not that of $\equiv SiOB(C_6F_5)_2$ or $\equiv SiOB(C_6H_5)_2$, the research of O'Hare and co-workers[19] is important. These authors prepared a silica-supported Lewis acid $\equiv SiOB(C_6F_5)_2$ surface and found the $^{11}$B CP MAS resonance at 2.34 ppm, not −0.44 ppm. The difference in $^{11}$B resonance positions for these two species is 2.78 ppm. This difference is almost double (1.5 ppm) that observed by replacing the 15 protons of $B(OC_6H_5)_3$ with F atoms to get $B(OC_6F_5)_3$.[31] It is concluded that the ca. 2.78 ppm difference observed between $^{11}$B resonances of **S3b** and $\equiv SiOB(C_6F_5)_2$ is significant enough to indicate that uncatalyzed dehydrocoupling did not occur during the preparation of **S3a** or **S3b**.

Additionally, the $^{31}$P CP MAS NMR of **S4a** and **S4b** were measured (Figure 1, bottom right, and Figures S6 and S7 in the Supporting Information). The strongest resonance was at 44.67 ppm (for **S4a**) and 62.57 ppm (for **S4b**), respectively. These resonances are those of the phosphorus bound to the nanosilica particles **S4a** and **S4b**. These resonances also exhibit spinning sidebands. They can be seen at ±(spinning rate of samples in zirconia rotor)/(instrument frequency for $^{31}$P) = 14000 Hz/162 MHz = ±86.4 ppm from the main $^{31}$P resonance. For **S4a** these are at ca. 131.1 and −41.7 ppm, respectively (Figure 1). Also observed in the $^{31}$P CP MAS spectrum of **S4a** is a resonance at ca. −5.6 ppm. This resonance position is mutually consistent with unreacted **2a** that remained adsorbed onto the nanosilica particles after the synthetic reaction to generate **S4a** was terminated (see Scheme 1, step 3). A solution $^{31}$P NMR spectrum of **2a** is shown in the inset of Figure 1 (bottom right). In the absence of nanosilica particles, the P atom of **2a** resonates at ca. −17.1 ppm. That a small portion of **2a** did not bind to **S1** was also confirmed by ATR FTIR (see text above and text associated with Figure 2). Finally, a peak was observed at ca. 27.5 ppm in the $^{31}$P CP MAS NMR of **S4**. This P resonance position is mutually consistent with a $P^{V}{=}O$ moiety and implies that, over time, some $P^{III}$ atoms of **4** become oxidized to $P^{V}$ and samples of **S4** should be stored under nitrogen. It should be

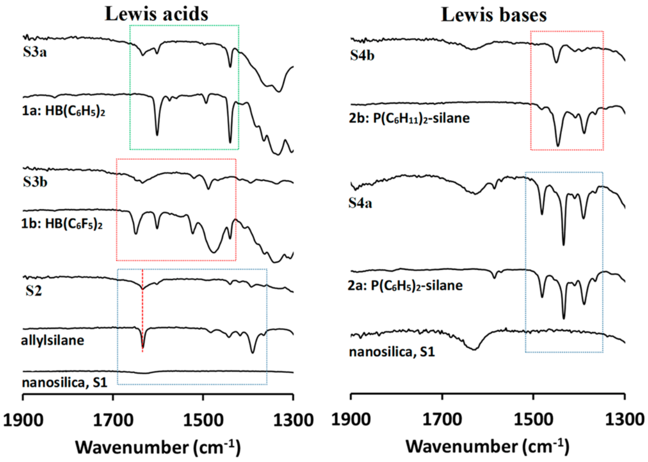

**Figure 2.** Comparative ATR FTIR spectra of surfaces **S1**−**S4** and their precursors **1** and **2**. The boxes highlight areas for comparison as follows. On the left, the C═C stretching vibration of allylsilane is present in **S2** but not in **S1**. The vibrational frequencies of **1a** and **1b** are also present in the ATR FTIRs of **S3a** and **S3b**, respectively. On the right, the frequencies of **2a** and **2b** are present in the ATR FTIRs of **S4a** and **S4b**, respectively. This indicates that allylsilane was successfully grafted onto **S1** to give **S2** and that **1** and **2** were successfully anchored onto **S3** and **S4**, as shown in Scheme 1.

noted that the quantity of $P^V$═O generation over 2 months when **S4** is stored under argon is so small that XPS measurements fail to detect it unambiguously (see text below and Figure 3).

**ATR FTIR.** Figure 2 shows ATR FTIR spectra in the 1300−1900 $cm^{-1}$ region, highlighting areas of interest for the functionalized surfaces **S2**−**S4** and their precursors. The C═C stretching frequency at 1633 $cm^{-1}$ (characteristic of an allyl functionality) and equivalent fingerprint region vibrational bands are present in the ATR FTIR spectra of both allyltriethoxysilane and **S2** but are absent in the ATR FTIR of nanopowder silica surface **S1**. This confirms the successful anchoring of the allylsilane on surface **S1**. The aromatic C═C stretching frequencies in the highlighted areas of the precursors **1a** and **1b** is slightly blue shifted in the supports **S3a** and **S3b**, which is consistent with successful hydroboration of the allyl moiety of **S2**.

A comparison of the ATR FTIR fingerprint region of the Lewis base precursor $(EtO)_3Si(CH_2)_2PR_2$ (**2a** with $PR_2$ = $P(C_6H_5)_2$ and **2b** with $PR_2$ = $P(C_6H_{11})_2$) hydroxylated nanopowder silica surface **S1** and supported Lewis base surfaces **S4a** and **S4b** shows the presence of stretching frequencies of the phosphine silanes **2** in the same region as for **S4**, but these were absent in **S1**. This confirms the anchoring of the phosphine silanes **2** onto **S1**.

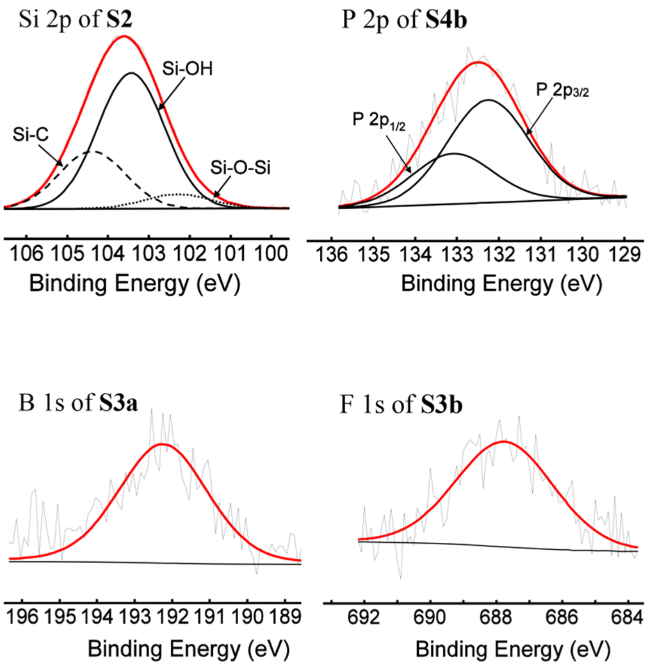

**Figure 3.** XPS spectra of the Si 2p area of **S2** indicating three different simulated Si species in the Si photoelectron envelope (top left), P 2p area of **S4b** indicating the simulated P $2p_{1/2}$ and P $2p_{3/2}$ components of P (top right), B 1s area of **S3a** (bottom left), and the F 1s area of **S3b** (bottom right). Additional XPS spectra may be found in Figures S8−S12 in the Supporting Information.

*X-ray Photoelectron Spectroscopy.* XPS was carried out for all of the supported Lewis acids and bases, with the aim of identifying and confirming the presence of specific elements on the surfaces. An XPS spectrum reveals the core level binding energies of all elements present in the surface region of a sample. These binding energies are sensitive to the oxidation state as well as the chemical environment of the atom. Adventitious oxygen and carbon are usually always present on all samples and are used to correct for any charging effects observed in all the measured photoelectron lines of importance. The binding energy of the simulated adventitious C 1s peak was set at 284.8 eV.[32]

As an example, the Si 2p area of **S2** is shown in Figure 3 (top left). Since the spin−orbit splitting between Si $2p_{3/2}$ and Si $2p_{1/2}$ is a small separation (Δ = 0.63 eV), it is considered unresolved and the spectrum is thus simulated with one peak. Experimentally, the measured full width at half-maximum (fwhm) of the Si 2p photoelectron lines was ca. 3.4 eV. Since Si 2p photoelectron lines of single Si species are associated with fwhm values of 1.9 eV,[33] it follows that there is more than one Si species present. The Si 2p envelope was therefore simulated to fit three identifiable Si species with each having a fwhm of 1.9 eV. The three fitted species are Si−O−Si from the silica nanoparticles themselves at the lowest binding energy of ca. 101.9 eV, Si−OH at ca. 102.9 eV, which are unreacted OH functionality remnants from **S1**, and the Si−C of the silane at the highest binding energy of ca. 104.1 eV. The ratio between the Si−OH and Si−C intensities indicates that ca. 23% of the available Si−OH functionalities on **S1** were used for anchoring allyltriethoxysilane to generate **S2**.

The P 2p photoelectron lines show the presence of a P(III) species, since the P $2p_{3/2}$ photoelectron line was found at ca. 131.8 eV with the P $2p_{1/2}$ photoelectron line being ca. 0.8 eV higher. Figure 3 (top right) shows the P 2p photoelectron lines of **S4b**. That minimal to no oxidation of the P to O═$P^V$ occurred within 1 month of preparation and storage under argon was deduced from the absence of a clear $P^V$═O photoelectron line (or even a clear shoulder) at ca. 134.5 eV[34] in the XPS spectra (see Figure 3 for **S4b**). However, $^{31}$P CP MAS NMR spectra obtained a few months after storing **S4a** and **S4b** showed that a small amount of $P^V$═O did form over time. It is concluded that it is best to store all surfaces under argon at low temperatures.

The B 1s photoelectron lines of **S3a** and **S3b** are present as broad peaks with low intensities. Figure 3 (bottom left) shows

Table 2. Summary of the Different Combinations of Supported and Associated (Solution Phase) Lewis Bases and Lewis Acids Used to form FLP/$CO_2$ Adducts on Surfaces S5 and S6, HCOOH Adsorbed on Surfaces S13 and S14 (Formed from S8 and S9) and diborano Formates Adsorbed on Surfaces S11 and S12[a]

| entry | solution-phase Lewis base **3**; $PR'_3$ | supported Lewis acid **S3** ((supp)-$BR_2$) | product; component sequence of Lewis adduct and captured $CO_2$; $\nu(C{=}O)/cm^{-1}$; int ratio[b] $\nu(CO_2)/\nu(\equiv Si{-}O{-}Si\equiv)$ (for $CO_2$ captured) | HCOOH on **S13** - prec no.; $\nu(C{=}O)/cm^{-1}$ on **S13**; **S13** int ratio[b] $\nu(C{=}O)/\nu(\equiv Si{-}O{-}Si\equiv)$ | product for HCOOH reaction with **3** and **S3** and/or **S8** rearrangement to form diborano formate surface **S11**; component sequence; $\nu(C{\cdots}O)/cm^{-1}$; int. ratio[b] $\nu(C{\cdots}O)/\nu(\equiv Si{-}O{-}Si\equiv)$ |
|---|---|---|---|---|---|
| 1 | **3a**; $P(C_6F_5)_3$ | **S3b** (R = $C_6F_5$) | **S5a**; **3a**$^{\oplus}$–COO–$^{\ominus}$**S3b**; 1643; 0.08 | **S8a**; 1739; 0.04 | **11a**; [**3aH**]$^{\oplus}$[**S3b**⋯O⋯CH⋯O⋯**S3b**]$^{\ominus}$; 1638;0.08 |
| 2 | **3b**; $P(C_6H_5)_3$ | **S3b** (R = $C_6F_5$) | **S5b**; **3b**$^{\oplus}$–COO–$^{\ominus}$**S3b**; 1634; 0.13 | **S8b**;1739; 0.04 | **11b**; [**3bH**]$^{\oplus}$[**S3b**⋯O⋯CH⋯O⋯**S3b**]$^{\ominus -}$; nd; nd |
| 3 | **3c**; $P(Mes)_3$ | **S3b** (R = $C_6F_5$) | **S5c**; **3c**$^{\oplus}$–COO–$^{\ominus}$**S3b**; nd; nd | **S8c**; 1739; 0.08 | **11c**; [**3cH**]$^{\oplus}$[**S3b**⋯O⋯CH⋯O⋯**S3b**]$^{\ominus}$; nd; nd |
| 4 | **3a**; $P(C_6F_5)_3$ | **S3a** (R = $C_6H_5$) | **S5d**; **3a**$^{\oplus}$–COO–$^{\ominus}$**S3a**; nd; nd | **S8d**; 1739; 0.05 | **11d**; [**3aH**]$^{\oplus}$[**S3a**⋯O⋯CH⋯O⋯**S3a**]$^{\ominus}$; 1640; 0.15 |
| 5 | **3b**; $P(C_6H_5)_3$ | **S3a** (R = $C_6H_5$) | **S5e**; **3b**$^{\oplus}$–COO–$^{\ominus}$**S3a**; 1631; 0.26 | **S8e**; 1739; 0.04 | **11e**; [**3bH**]$^{\oplus}$[**S3a**⋯O⋯CH⋯O⋯**S3a**]$^{\ominus}$; nd; nd |
| 6 | **3c**; $P(Mes)_3$ | **S3a**;(R = $C_6H_5$) | **S5f**; **3c**$^{\oplus}$–COO–$^{\ominus}$**S3a**; nd; nd | **S8f**; 1739; 0.04 | **11f**; [**3cH**]$^{\oplus}$[**S3a**⋯O⋯CH⋯O⋯**S3a**]$^{\ominus}$; nd; nd |
| entry | supported Lewis base **S4** ((supp)-$PR_2$) | solution-phase Lewis acid **4**; $BR_3$ | product; component sequence of Lewis adduct and captured $CO_2$; $\nu(C{=}O)/cm^{-1}$; int. ratio[b] $\nu(CO_2)/\nu(\equiv Si{-}O{-}Si\equiv)$ (for $CO_2$ capture) | HCOOH on **S14** - prec. no.; $\nu(C{=}O)/cm^{-1}$on **S14**; **S14** int. ratio[b] $\nu(C{=}O)/\nu(\equiv Si{-}O{-}Si\equiv)$ | product for HCOOH reaction with **4** and **S4** and/or **S10** rearrangement to form diborano formate surface **S12**; component sequence; $\nu(C{\cdots}O)/cm^{-1}$; int. ratio[b] $\nu(C{\cdots}O)/\nu(\equiv Si{-}O{-}Si\equiv)$ |
| 7 | **S4a** (R = $C_6H_5$) | **4a**; $B(C_6F_5)_3$ | **S6a**; S4a$^{\oplus}$–COO–$^{\ominus}$**4a**; 1642; 0.25 | **S10a**; nd; nd | **12a**; [**S4aH**]$^{\oplus}$[**4a**(C⋯O)/O⋯CH⋯O⋯**4a**]$^{\ominus}$; nd; nd |
| 8 | **S4a** (R = $C_6H_5$) | **4b**; $B(C_6H_5)_3$ | **S6b**; **S4a**$^{\oplus}$–COO–$^{\ominus}$**4b**; 1632; 0.14 | **S10b**; 1738; 0.19[b] | **12b**; [**S4aH**]$^{\oplus}$[**4b**⋯O⋯CH⋯O⋯**4b**]$^{\ominus}$; 1639; 0.5 |
| 9 | **S4a** (R = $C_6H_5$) | **4c**; $B(Mes)_3$ | **S6c**; **S4a**$^{\oplus}$–COO–$^{\ominus}$**4c**; nd; nd | **S10c**; 1738; 0.06 | **12c**; [**S4aH**]$^{\oplus}$[**4c**⋯O⋯CH⋯O⋯**4c**]$^{\ominus}$; nd; nd |
| 10 | **S4b** (R = $C_6H_{11}$) | **4a**; $B(C_6F_5)_3$ | **S6d**; **S4b**$^{\oplus}$–COO–$^{\ominus}$**4a**; 1643; 0.17 | **S10d**; 1739; 0.03 | **12d**; [**S4bH**]$^{\oplus}$[**4a**⋯O⋯CH⋯O⋯**4a**]$^{\ominus}$; 1640; 0.02 |
| 11 | **S4b** (R = $C_6H_{11}$) | **4b**; $B(C_6H_5)_3$ | **S6e**; **S4b**$^{\oplus}$–COO–$^{\ominus}$**4b**; 1634; 0.08 | **S10e**; 1739; 0.09 | **12e**; [**S4bH**]$^{\oplus}$[**4b**⋯O⋯CH⋯O⋯**4b**]$^{\ominus}$; 1640; 0.03 |
| 12 | **S4b** (R = $C_6H_{11}$) | **4c**; $B(Mes)_3$ | **S6f**; **S4b**$^{\oplus}$–COO–$^{\ominus}$**4c**; nd; nd | **S10f**; nd; nd | **12f**; [**S4bH**]$^{\oplus}$[**4c**⋯O⋯CH⋯O⋯**4c**]$^{\ominus}$; nd; nd |

[a] ATR FTIR carbonyl stretching frequency data are also summarized (nd = not detected, int = intensity, prec = precursor). [b] Intensity ratio = [intensity of absorbed $CO_2$ stretching vibration (or HCOOH $\nu(C{=}O)$ or diborano formate $\nu(C{\cdots}O)$]/(intensity of support ($\equiv$Si–O) asymmetric stretching vibration). The highest ratio indicates the most successful $CO_2$ absorption, HCOOH conversion, or diborano formate formation. Because the largest intensity ratio of (intensity of HCOOH $\nu(C{=}O)$ vibration)/(intensity of the support silica $\nu(\equiv Si{-}O{-}Si\equiv)$ vibration) = 0.19 was observed for surface **S14** originating from precursor surface **S10b** (entry 8 above, see also Scheme 3 for structures), this was the most successful FLP system for the reduction of $CO_2$ to formic acid.

the B 1s spectrum of **S3a** as an example and indicates the presence of a B(III) species at 192.2 eV with a fwhm value of 2.8 eV. The B 1s photoelectron line of **S3b** appears at a higher binding energy (193.9 eV), due to the influence of the electron-withdrawing fluorine atoms of the $C_6F_5$ moieties.

A symmetrical F 1s photoelectron line was simulated at 687.8 eV (Figure 3, bottom right) for surface **S3b**, which is the characteristic position of organic fluorines.[35,36]

The XPS, ATR FTIR, and solid-state NMR spectra of the supported phases **S2**–**S4** all confirm that anchoring of the Lewis acids **1a** and **1b** and Lewis bases **2a** and **2b** onto the functionalized silica nanopowder has been achieved.

**$CO_2$ Capture.** Due to the inability of frustrated Lewis pairs (FLPs) to form a normal Lewis adduct, it has the unique ability to capture small molecules such as $CO_2$, convert it, for example, to HCOOH, and release the converted products. Here, a suspension of supported Lewis acid **S3a** or **S3b** or supported Lewis base **S4a** or **S4b** was combined with solution-phase Lewis bases **3a**–**c** or Lewis acids **4a**–**c** as FLP partners with the aim of finding combinations that will lead to the most successful capture of $CO_2$. Table 2 summarizes the different combinations tested. The reactions that takes place to form the different (Lewis base)–COO–(Lewis acid) adducts are shown in Scheme 2. The resulting adducts **S5** and **S6** were analyzed by ATR FTIR at both low (−64 °C) and room temperature. As a control, pure hydroxylated silica nanopowder **S1** (used as the FLP/$CO_2$ support precursor) was first tested for its ability to capture $CO_2$ under the same conditions used for the FLP systems. ATR FTIR measurements on the control could not detect any trapped or captured $CO_2$ (see Figure S17 in the Supporting Information).

Figure 4 shows the ATR FTIR spectra of the FLP/$CO_2$ system **S5e** as an example at −64 °C and at room temperature. The $CO_2$ captured by **S5e** is indicated by the characteristic C=O stretching frequency found at ca. 1631 $cm^{-1}$. The C=O stretching frequency for captured $CO_2$ using different FLPs differs depending on the Lewis acid and base used. For example, Zhao and Stephan[37] found that for the FLP/$CO_2$ system $P^tBu_3$-$CO_2$-$B(C_6F_5)_3$, $\nu(C{=}O)$ was 1695 $cm^{-1}$, while for $(Mes)_2P$-$(CH_2)_2B(C_6F_5)_2$-$CO_2$, it was found at 1694 $cm^{-1}$. In contrast, $\nu(C{=}O)$ of captured $CO_2$ using the bis-borane $Me_2C{=}C(B(C_6F_5)_2)_2$ or $Me_2C{=}C(BCl_2)_2$ and $P^tBu_3$ was found at 1608 and 1617 $cm^{-1}$, respectively.[37,38] The carbene FLP $PhCH_2NMe_2(CO_2)B(C_6F_5)_3$ resulted[38] in $\nu(C{=}O)$ 1822 $cm^{-1}$, while the ruthenium-containing FLP $[N\text{-}((CH_2)_2NHP^iPr_2)_2((CH_2)_2NP(CO_2)^iPr_2)Ru][BPh_4]$ showed $\nu(C{=}O)$ at 1651 $cm^{-1}$ after $CO_2$ capture.[38] For complexes **S5** we found $1631 \leq \nu(C{=}O) \leq 1643$ $cm^{-1}$ (Table 2).

Comparison of the ATR FTIR spectra of **S5** and **S6** measured at −64 °C (directly after exposure to 2 bar of $CO_2$) with the

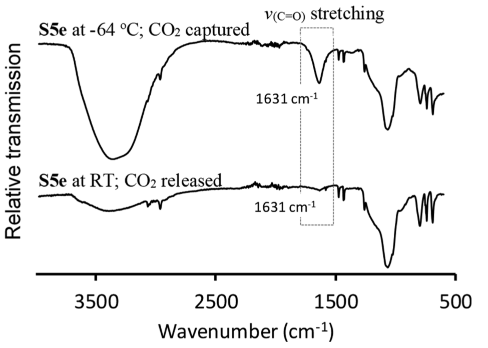

**Figure 4.** ATR FTIR spectra of the FLP/$CO_2$ system **S5e** at −64 °C (top) recorded within 5 min of exposure to 2 bar $CO_2$ and (bottom) at room temperature (RT) after 15 min of exposure to the atmosphere. The $\nu$(C═O) vibrational band at 1631 $cm^{-1}$ disappeared, indicating that $CO_2$ was released at room temperature.

spectrum at room temperature after 15 min of exposure to the atmosphere (Figure 4 shows this for **S5e**) showed that the $\nu$(C═O) vibrational band disappears at higher temperatures. This indicates that $CO_2$ is released at higher temperatures.

In an effort to determine the relative efficiency of $CO_2$ capture with the different FLP/$CO_2$ systems **S5** and **S6**, the intensity ratios between the $CO_2$ stretching frequency (at ca. 1631−1643 $cm^{-1}$) and the characteristic ≡Si−O−Si≡≡ asymmetric stretching vibrations (in the 900−1300 $cm^{-1}$ area) of the support were determined and compared (Table 2). The highest ratios, indicating the most effective $CO_2$ captures, were obtained with **S5e** and **S6a**. Both contain a Lewis base with phenyls, either $P(C_6H_5)_3$ or $P(C_6H_5)_2$. It follows that a phenyl-containing phosphine is the most effective Lewis base for the purpose of $CO_2$ capture in the compound series reported here.

Despite **3c** with its three electron-donating methyl substituents on the phenyl ring being a stronger Lewis base than **3b**, FLP systems **S5c** and **S5f** as well as **S6c** and **S6f**, containing either a Lewis acid or Lewis base with mesityl groups, did not show measurable $CO_2$ capture. This may be attributed to the steric bulk of the mesityl groups. Using the Tolman cone angle, $\theta$, as a measure of bulkiness, the Lewis bases **3** decrease in size in the order $P(Mes)_3$ ($\theta$ = 212°) > $P(C_6F_5)_3$ ($\theta$ = 184°) > $P(C_6H_5)_3$ ($\theta$ = 145°).[39,40] The greater the Tolman cone angle, the bulkier the phosphine. The steric hindrance the large trimesitylphosphine imposes on the FLPs blocks $CO_2$ access to the P center of the Lewis base and explains the inability of these FLPs to capture $CO_2$. On comparison of $P(C_6F_5)_3$ and $P(C_6H_5)_3$ Lewis bases **3a** and **3b**, $P(C_6H_5)_3$ has the smallest Tolman cone angle ($\theta$ = 145°). When $P(C_6H_5)_3$ (**3b**) was combined with **S3a** (which contains the $CH_2CH_2B(C_6H_5)_2$ molecular fragment) to give **S5e**, the most effective $CO_2$ capture was observed (Table 2, entry 5, intensity ratio $\nu(CO_2)/\nu$(≡Si−O−Si≡) = 0.26). In contrast, when $P(C_6F_5)_3$ (**3a**) was combined with **S3a** containing a $CH_2CH_2B(C_6H_5)_2$ molecular fragment (Table 2, entry 4), no $CO_2$ capture was observed at all because no $\nu$(C═O) could be detected. This means **S 5d** does not form.

Combining $P(C_6F_5)_3$ (**3a**) with **S3b** ($B(C_6F_5)_2$; Table 2, entry 1) resulted in limited efficiency for $CO_2$ capture as indicated, by the intensity ratio $\nu(CO2)/\nu$(≡Si−O−Si≡) of 0.08 for **S5a** (entry 1). This happens because the electron-withdrawing fluorine results in a Lewis base, **3a**, with an electron-poor P center (a weak Lewis base), which cannot effectively donate electrons to the $\delta^+$ C atom of $CO_2$. The B center of the fluorine-containing Lewis acid $B(C_6F_5)_3$ is also electron-poor. However, this results in the boron being more susceptible to attack by the electron-rich O of $CO_2$. This affords better $CO_2$ capturing capabilities in FLP systems, as observed in **S5a**, **S5b**, and **S6b**. The stronger Lewis acidity of **4a**, $B(C_6F_5)_3$, and small Tolman cone angle for phenylphosphines in **S4a** also explains the good $CO_2$ capture by **S6a** (entry 7).

The relatively poor $CO_2$ capture capability of **S6e** (entry 11, Table 2, intensity ratio $\nu(CO_2)/\nu$(≡Si−O−Si≡) of 0.08) indicates that the phosphine **S4b** with R = $C_6H_{11}$ is also more sterically crowded than $C_6H_5$-containing phosphines such as **S5e** (entry 5) and **S6b** (entry 8).

For application in carbon capture and storage technologies it is essential that materials not only bind but also readily release $CO_2$. To this end we measured the ATR FTIR spectra of all $CO_2$-exposed systems in Table 2 after warming to room temperature. As an example, Figure 4 shows that FLP system **S5e**, which displays the highest uptake of $CO_2$ at −64 °C, released all adsorbed $CO_2$ within 15 min of exposure to the atmosphere at room temperature. All other systems in Table 2, which adsorbed $CO_2$ at low temperature, showed the same behavior.

**$CO_2$ Conversion.** One of the easiest ways to reduce $CO_2$ is the incorporation of a hydride at the carbonyl carbon, $H^-$···$CO_2$, and a proton at one of the carbonyl oxygens, $H^+$···OCO, to ultimately produce formic acid, HCOOH. The proton and hydride can be generated by the heterolytic dissociation of $H_2$ using an FLP.[13,41] According to calculations by Ye and co-workers,[42−44] activation of $H_2$ by dissociative adsorption before $CO_2$ addition leads to a lower energy pathway for hydrogenation of $CO_2$ in comparison to that by reacting $H_2$ with chemisorbed $CO_2$. In addition, chemisorbed $CO_2$ leads to unfavorable intermediates, such as Lewis base bound HCO and Lewis acid bound OH. Another advantage of starting with $H_2$ activation en route to $CO_2$ reduction is that $H_2$ can be activated (cleaved to $H^-$ and $H^+$) by FLPs at room temperature and $CO_2$ can be reduced at 60 °C. This eliminates the need to use low temperatures.[45]

The two-step procedure used for the conversion of $CO_2$ to HCOOH utilizing supported Lewis acids/bases, **S3**/**S4**, and dissolved Lewis bases/acids, **3**/**4**, are shown in Scheme 3 (reaction A).

At the end of the reduction of $CO_2$ with $H_2$ using FLPs according to Scheme 3, the supported Lewis acid/base was separated from the solution phase for ATR FTIR analysis and $^{13}C$, $^{11}B$, and $^{31}P$ CP MAS NMR to identify HCOOH and any other products that may have formed on the surface.

By way of an example, Figure 5 compares the ATR FTIR spectra of neat liquid formic acid on the ATR FTIR's diamond crystal, formic acid adsorbed onto nanopowder silica surface **S1**, supported Lewis acid **S8a** (see Scheme 3 for the structure) after $H_2$ activation and exposure to $CO_2$ at 60 °C, and **S5a** (see Scheme 2). With the exception of the spectrum of **S5a**, a carbonyl stretching frequency is observed in each spectrum in the wavenumber range 1689 ≤ $\nu$(C═O) ≤ 1739 $cm^{-1}$. Neat formic acid's $\nu$(C═O) measured directly on the crystal of an ATR FTIR (Figure 5, bottom) was measured at 1689 $cm^{-1}$. This is well within the literature range of ca. 1685−1693 $cm^{-1}$.[46−48] When we adsorbed formic acid onto nanopowder silica surface **S1**, the $\nu$(C═O) band of HCOOH was found at 1729 $cm^{-1}$. This correlates well with reported $\nu$(C═O) values of adsorbed formic acid on different silica supports: viz., 1725−1727 $cm^{-1}$ for $SiO_2$[49,50] and 1717 $cm^{-1}$ for potassium-promoted Cu/

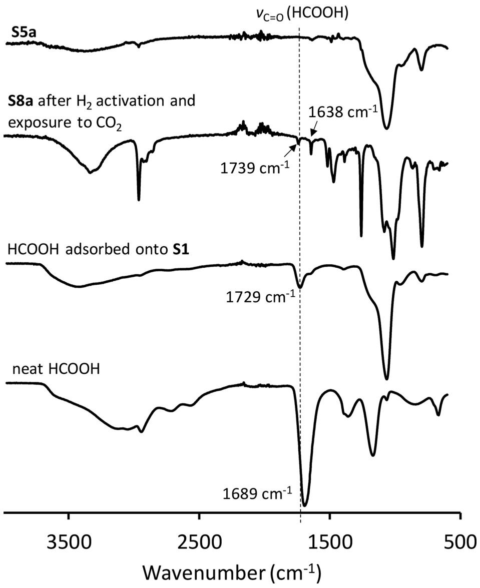

**Figure 5.** ATR FTIR spectra of (from top to bottom) **S5a** (Scheme 2), **S8a** after exposure of a mixture of **S3b** and **3a** first to $H_2$ and then $CO_2$ (**S8a** converted to **S13** with fragments of **S11a** on it according to Scheme 3), neat HCOOH adsorbed onto nanopowder silica surface **S1**, and neat formic acid on the ATR FTIR crystal at room temperature.

$SiO_2$.[51] The results are consistent with $\nu$(C=O) of HCOOH being blue-shifted upon adsorption onto a silica-based support.

The spectrum of **S5a** (Figure 5, top) was recorded at room temperature. At this temperature, $CO_2$ is released, and one is left with only a spectrum of the precursor Lewis acid support **S3b** and the associated Lewis base **3a** (see Scheme 2 for the formation of **S5a** from **S3b** and the release of $CO_2$ at room temperature).

The ATR FTIR spectrum of **S8a** (Figure 5, second from the top), a sample of which is obtained after $H_2$ activation over **S3b**/**3a** and subsequent exposure to $CO_2$ (Scheme 3), showed stretching frequencies at 1638 and 1739 cm$^{-1}$ which are absent in the spectrum of **S5a**. The 1638 cm$^{-1}$ vibration is, in agreement with research performed by Stephan and co-workers,[45] assigned to a diborano formate species, [**3aH**]$^{\oplus}$[**S3b**⋯O⋯CH⋯O⋯**S3b**]$^{\ominus}$ (**S11a**) and will be discussed below.

The 1739 cm$^{-1}$ vibration is not associated with $CO_2$ capture, since $\nu$(C=O) of captured $CO_2$ appears at 1631 cm$^{-1}$ (Figure 4). From the proposed path in Scheme 3 to obtain HCOOH, two possible structures exist that may be the origin of the 1739 cm$^{-1}$ vibration. It belongs to either free formic acid adsorbed on the surface of the support (Scheme 3, structure **S13**) or formic acid which is still associated within the FLP, as shown in Scheme 3 by **S8**. There are no literature ATR FTIR spectra for formic acid associated with surface-bound FLPs available for a comparison of $\nu$(C=O) band positions. Because the C=O vibration of $[(C_6F_5)_2RB{-}OCOH]^-$ is reported to be at ca. $\nu$(C=O) 1684 cm$^{-1}$,[52] the vibration at 1739 cm$^{-1}$ is not considered to be related to the mono borano ester of formic acid that is still associated with the FLP **S8**. However, the $\nu$(C=O) of HCOOH absorbed on a hydroxylated nanosilica surface, **S1**, was measured during this study at 1729 cm$^{-1}$ (see Figure 5, second from the bottom). It appears that the presence of the supported Lewis borane base on **S13** shifted the HCOOH C=O vibrational band via a nonspecific interaction to 1729 cm$^{-1}$. The important conclusion from these results is that the appearance of the $\nu$(C=O) 1739 cm$^{-1}$ vibrational band proves that $CO_2$ was reduced with $H_2$ to form formic acid according to Scheme 3. This conclusion is also supported from results obtained by $^{13}$C and $^{11}$B CP MAS NMR experiments, which will be discussed below.

Having established that all surface-bound Lewis acid/solution-phase Lewis base FLPs **S8** can reduce $CO_2$ to HCOOH, attention was focused on the surface-bound Lewis base/solution-phase Lewis acid systems **S10** (Scheme 3, bottom). Figure 6 compares the ATR FTIR spectra of **S6b** (top) at room temperature (i.e., $CO_2$ was released at room temperature according to Scheme 2, leaving behind **S4a** and **4b** on the nanopowder silica surface) with **S10b** (second from the top) after exposure to $H_2$ and $CO_2$ according to Scheme 3, HCOOH adsorbed onto nanoparticle silica surface **S1** (second from the bottom), and neat HCOOH on an ATR FTIR diamond crystal (bottom).

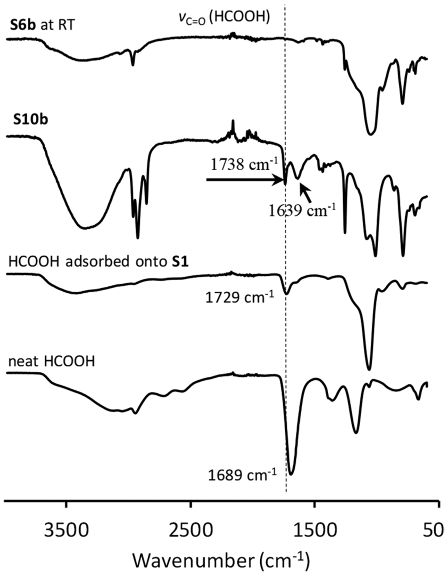

**Figure 6.** ATR FTIR spectra of (top) **S6b** at RT, i.e. $CO_2$ was released according to Scheme 2; (second from the top) **S10b** after exposure to $H_2$ and $CO_2$, i.e. surface **S14** was generated; (second from the bottom) neat HCOOH adsorbed onto nanopowder silica surface **S1**; (bottom) neat HCOOH on an ATR crystal.

Just as analyses of the FLP system **S8a** showed traces of diborano formate complexes **S11a** (see above and Scheme 3, top), the FLP system **S10b**, after dissociation of $H_2$ and subsequent exposure to $CO_2$, showed in addition to the C=O vibration of the HCOOH that formed at $\nu$(C=O) 1738 cm$^{-1}$, also the $\nu$(C⋯O) stretching frequency of the diborano formate **S12b**, [**S4aH**]$^{\oplus}$[**4b**⋯O⋯CH⋯O⋯**4b**]$^{\ominus}$ at 1639 cm$^{-1}$. This vibrational band is at the same stretching frequency found for the purposefully prepared diborano formate surface **S12b** (reaction B in Scheme 3; see also section on diborano formates below) and parallels results described by Stephan.[45]

The intensity ratio between the carbonyl stretching frequency, $\nu$(C=O) at 1739 cm$^{-1}$, of the formed formic acid on **S14** and the characteristic ≡Si−O−Si≡ asymmetric stretching vibrations (in the 900−1300 cm$^{-1}$ area) of the silica nanoparticle and the intensity ratio between the $\nu$(C⋯O) of the diborano formate at ca. 1640 cm$^{-1}$ and the characteristic ≡Si−O−Si≡ asymmetric stretching vibrations are summarized in Table 2. These data are used as a measure of the effectiveness of $H_2$ activation and $CO_2$ reduction to formic acid as well as for the reaction between the formed HCOOH and free **S3** to generate the diborano formate by the 12 tested surfaces **S8a–f** and **S10a–f**. For **S10b**, the intensity ratio $\nu$(C=O)/$\nu$(≡Si–O–Si≡) of 0.19 (Table 2) for the formed formic acid carbonyl stretching vibration at $\nu$(C=O) 1739 $\text{cm}^{-1}$ is 2–6 times larger than all other ratios for detected HCOOH formation by the other FLP systems that we studied. This indicated this FLP surface generated the largest quantity of HCOOH upon $CO_2$ reduction in the compound series we studied. **S10b** is also the surface that resulted in the highest conversion of the associated formic acid to the diborano formate. Only **S10a** and **S10f** of all 12 FLPs tested failed to show the HCOOH carbonyl stretching vibration at ca. 1739 $\text{cm}^{-1}$. This resulted in an intensity ratio of (intensity of HCOOH C=O vibrational band)/(intensity of (≡Si–O–Si≡ vibrational band) = 0 and implied that all of the FLP systems except these two were able to dissociate $H_2$ and subsequently hydrogenate $CO_2$ to form HCOOH.

It is instructive to note that ATR FTIR measurements detected the formation of small quantities of diborano formate side products **S11a**, **S11d**, **S12b**, **S12d**, and **S12e** during the analyses of **S8** and **S10**, but not **S11b**, **S11c**, **S11e**, **S11f**, **S12a**, **S12c**, and **S12f** after treatment of FLP systems **S3**/**3** and **S4**/**4** with $H_2$ and $CO_2$. To understand this result more, the diborano formate surfaces **S11** and **S12** were purposefully prepared and analyzed.

**Diborano Formate Systems S11 and S12.** As discussed above, synthesis of HCOOH via **S8** and **S10** in selected cases also gave the diborano formate systems **S11** and **S12** as side products. To unambiguously confirm the identification of **S11** and **S12** side products and to understand the spectroscopic properties of these formates better, they were also synthesized in a dedicatedly fashion by treating the FLP systems **S3**/**3** and **S4**/**4** with a ca. 50-fold excess of HCOOH (Scheme 3, reaction B on the right). In terms of the **S3**/**3** system, only **3a** reacted with **S3a** and **S3b** to give **S11a** and **S11d**. Compounds **3b** and **3c** proved to be unreactive under these conditions and hence failed to generate **S11b**, **S11c**, **S11e**, and **S11f**. Similarly, in terms of the **S4**/**4** system, compound **4c** reacted with neither **S4a** nor **S4b**, and hence **S12c** and **S12f** could not be generated. Compound **4b** reacted with both **S4a** and **S4b** to generate **S12b** and **S12e**, respectively. Compound **4a** reacted with **S4b** but not **S4a**, and hence **S12d** was generated, but not **S12a** (Scheme 3, reaction B). It is satisfying to observe that the forced, dedicated attempts to synthesize **S11** and **S12** according to reaction B in Scheme 3 succeeded or failed for the same surfaces for which diborano formates were detected as fortuitous side products during the synthesis of **S13** and **S14** according to reaction A in Scheme 3. ATR FTIR as well as $^{13}$C, $^{11}$B, and $^{31}$P CP MAS spectra are discussed below.

*ATR FTIR Measurements for S11 and S12.* Table 2 summarizes ATR FTIR $\nu$(C$\underline{\cdots}$O) stretching frequencies of the obtained diborano formate systems; all were in the range 1638–1640 $\text{cm}^{-1}$. Figure 7 shows both the ATR FTIR spectra of **S11a** ([**3aH**]$^{\oplus}$[**S3b**$\underline{\cdots}$O$\underline{\cdots}$CH$\underline{\cdots}$O$\underline{\cdots}$**S3b**]$^{\ominus}$) and **S12b** ([**S4aH**]$^{\oplus}$[4b$\underline{\cdots}$O$\underline{\cdots}$CH$\underline{\cdots}$O$\underline{\cdots}$**4b**]$^{\ominus}$._ $\nu$(C$\underline{\cdots}$O) vibrations at 1638 and 1639 $\text{cm}^{-1}$ were observed respectively (Table 2).

Stephan et al.[45] reported infrared data for a series of FLPs, [$^{t}Bu_3PH$][$RBH(C_6F_5)_2$], after reaction with HCOOH. They showed that the $\nu$(C$\underline{\cdots}$O) band of their obtained diborano formates, [$((C_6F_5)_2BR)_2(\mu\text{-}HCO_2)$][$t Bu_3PH$], was located at 1631–1638 $\text{cm}^{-1}$. Since the C$\underline{\cdots}$O band that appeared at 1638 or 1639 $\text{cm}^{-1}$ in the ATR FTIR spectra of **S11a** and **S12b**, were mutually consistent with those of Stephan, observations of these bands are considered the first indication that these diborano formates of the structure indicated in Scheme 3 formed. More importantly, we observe that **S11** and **S12** only formed when FLP systems **S3**/**3** and **S4**/**4** were treated with $H_2$ followed by $CO_2$ if at least **S8** and **S10** also formed. Although, **S11** and **S12** may be formed via a rearrangement process of **S8** and **S10** (Scheme 3), this rearrangement route is not favored by the authors. More likely, **S11** and **S12** formed according to reaction B in Scheme 3 only after HCOOH was formed via dissociation of **S8** and **S10** to liberate either HCOOH as the free acid or adsorbed on **S13** or **S14**.

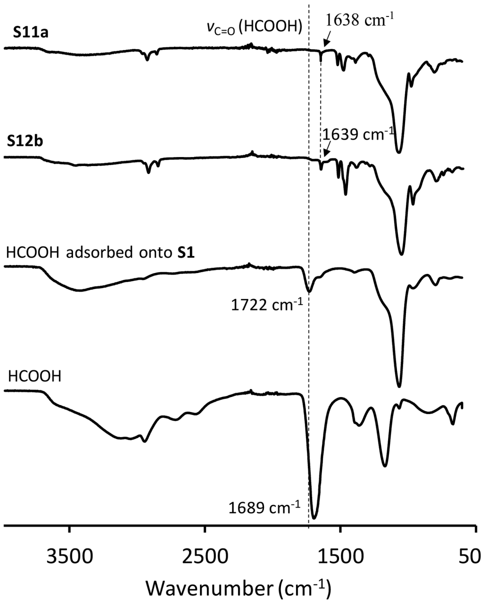

**Figure 7.** ATR FTIR spectra of (top) **S11a**, (second from the top) **S12b**, (second from the bottom) neat HCOOH adsorbed onto nanopowder silica surface **S1**, and (bottom) neat HCOOH on an ATR diamond crystal.

A possible mechanism by which this can happen is shown in Scheme 4.

Two important points stem from Scheme 4. **S11** can only form if two immobilized borano fragments on **S3** are close enough to each other so that HCOOH can access them both simultaneously. Being immobilized hampers this, and not all HCOOH will convert to the diborano formate **S11**. This explains why the present immobilized heterogeneous FLP systems are capable of releasing HCOOH, while the soluble FLPs studied by Stephan[45] did not; they converted all to diborano formates. In addition, the mere observation of fragments of **S11** and **S12** provides further evidence that the systems **S3**/**3** and **S4**/**4** can reduce $CO_2$ to formic acid because **S11** and **S12** would not form under our conditions if HCOOH did not form and were released from supports **S8** and **S10** first.

*$^{13}$C Solid-State NMR for S11 and S12.* The dedicated synthesized nanopowder silica surfaces **S11** and **S12** were also analyzed by $^{13}$C solid-state NMR. Figure 8 shows these spectra for **S12e** and **S11a**.

Consistent with data reported by Stephan and co-workers,[45] who reported a $^{13}$C resonance for the C$\underline{\cdots}$O fragment at 173.4 ppm for [$((C_6F_5)_2BR)_2(\mu\text{-}HCO_2)$][$t Bu_3PH$] complexes, a $^{13}$C C$\underline{\cdots}$O resonance at ca. 165–170 ppm was detected for **11a** and **12e**. This is the second spectroscopic evidence for the assignment of diborano formate structures as in Scheme 3. Once again, as described in the ATR FTIR section above,

**Scheme 4. Mechanism for the Formation of S11 after HCOOH Has Formed during Reaction A of Scheme 3**

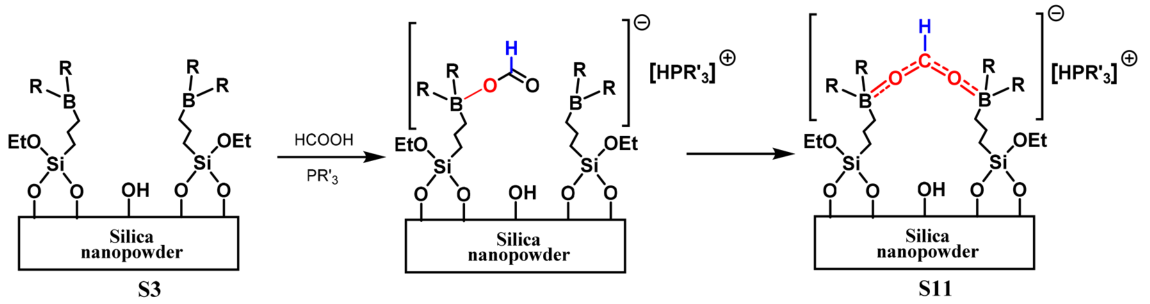

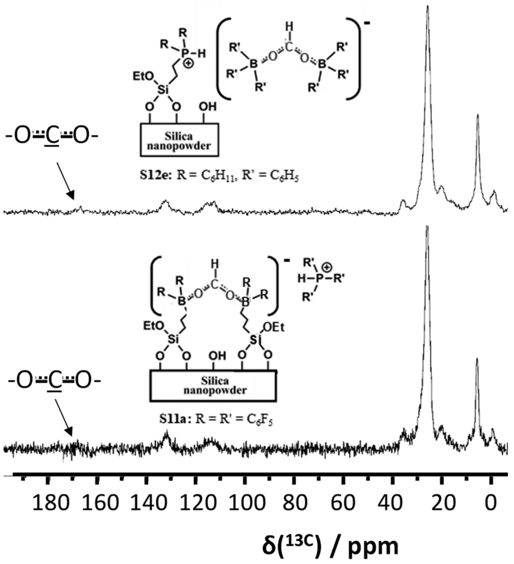

**Figure 8.** $^{13}$C solid-state NMR of **S12e** (top) and **S11a** (bottom). These two surfaces were purposefully prepared by the reaction between externally added HCOOH and either **S4b**/**4b** or **S3b**/**3a**. See Figures S26 and S27 in the Supporting Information for enlarged inserts of the 165−168 ppm range.

observation of the diborano formate $^{13}$C C$\underline{\cdots}$O resonances at ca. 165−168 ppm is only possible if the **S3**/**3** and **S4**/**4** FLP systems can reduce CO$_2$ to formic acid.

***$^{11}$B CP MAS Spectra of 3b and S11a.*** Clear evidence for the structures of **S11** and **S12** having been obtained, the $^{11}$B CP MAS NMR spectra of **S11** and **S12** are of interest. The $^{11}$B CP MAS NMR of reactant surface **S3b** is shown in Figure 9 (top left). The key $^{31}$B resonance for this surface is at −0.44 ppm, as discussed before (see text associated with Figure 1). Figure 9 (bottom left) shows the $^{11}$B CP MAS NMR of **S11a**. Three resonances are observed. The middle resonance is at −0.40 ppm and corresponds to unreacted **S3b**. The mere observation of this resonance bears testimony to just how frustrated the immobilized boranes on the nanopowder silica surfaces are. If both partners of the FLP were in solution, no unreacted **S3b** would be expected, as solution-phase studies elegantly showed.[45]

The appearance of a new resonance to the left of the middle resonance at 12.38 ppm is assigned to the diborano formate and parallels the $^{11}$B resonance positions for the diborano formates $[((C_6F_5)_2BR)_2(\mu\text{-}HCO_2)][t\text{Bu}_3PH]$, which were reported at 5.11 ppm.[52] The third resonance at −12 ppm was unexpected. This resonance position is characteristic of a $R_4B^+$ species.[53] On the basis of this evidence it is concluded that, although most borane fragments on **S3** are very sheltered and not easily accessible by the phosphine FLP partner **3**, there must be some that are more "naked" than others. Since the FLP partner in this case was PPh$_3$ (**3a**), which in itself is not a "highly" hindered phosphine, the formation of small quantities of a normal Lewis acid−base adduct, here **S3b**$^{\ominus}$−**3a**$^{\oplus}$, appears to be feasible. On the basis of this observation it is concluded that the more hindered the supported Lewis acid (or Lewis base) and its FLP partner, the dissolved Lewis base (or Lewis acid), are, the less FLP activity would be lost due to formation of catalytically "dead" Lewis adducts. The results summarized in Table 2 elegantly demonstrate this. All FLP systems that consisted of a B(Mes) or P(Mes) component (entries 3, 6, 9, and 12) failed to generate diborano formates **S11** and **S12** in detectable quantities. However, entry 12, which summarized results for the most frustrated FLP system consisting of **S4b** (R = C$_6$H$_{11}$) and **4c**, B(Mes)$_3$, waved a red flag. This system was so hindered that it also failed to generate HCOOH and failed to capture CO$_2$. It is concluded that an optimum degree of hindrance will exist for each application of an FLP.

***$^{31}$P CP MAS Spectra of S4b and S12e.*** Since the $^{11}$B CP MAS NMR spectra of **S11a** showed appreciable quantities of unreacted **S3b** in a sample of **S11a**, it follows that such a sample may also have some unreacted phosphine as well. The $^{31}$P CP MAS NMR spectrum of **S12e** showed two resonances (Figure 9, right bottom). The resonance at 33.4 ppm is assigned to the surface-bound $-PH(C_6H_{11})_2^{\oplus}$ (**H4b$^+$**), a FLP partner of the associated diborano formate fragment of **S12e**. The resonance at 59.2 ppm of **S12e** by comparison with the $^{31}$P CP MAS NMR resonance of **S4b** at 62.5 ppm in Figure 9 (right top) corresponds to unreacted supported Lewis base fragments of **S4b** on **S12e**. The upfield shift of this resonance of **S12e** in comparison to the analogous S4**b** resonance is mirrored by the upfield shift of PPh$_3$ at 10.5 ppm[54] and $[HPPh_3]^+$ at 8.0 ppm.[55]

## ■ CONCLUSIONS

Supported Lewis acids bases can be prepared by grafting the appropriate Lewis acid or Lewis base functionalized triethoxysilanes onto hydroxylated silica nanopowder. At least one but not all three of the ethoxy groups are split out as ethanol to generate a (silica surface Si)−O−Si−(spacer)−(Lewis acid/base) bond. This covalent anchoring method is strong enough to generate associated supported frustrated Lewis pairs that at −64 °C, in the absence of water and oxygen, can capture and retain CO$_2$ as a FLP-CO$_2$ adduct on the nanopowder silica surface. CO$_2$ may again be released at room temperature. Ten out of the 12 nanopowder silica-supported FLP systems tested were capable of dissociating and activating H$_2$ and subsequently hydrogenate CO$_2$ to form HCOOH, thereby demonstrating the success of heterogeneous FLP reduction of CO$_2$ to HCOOH.

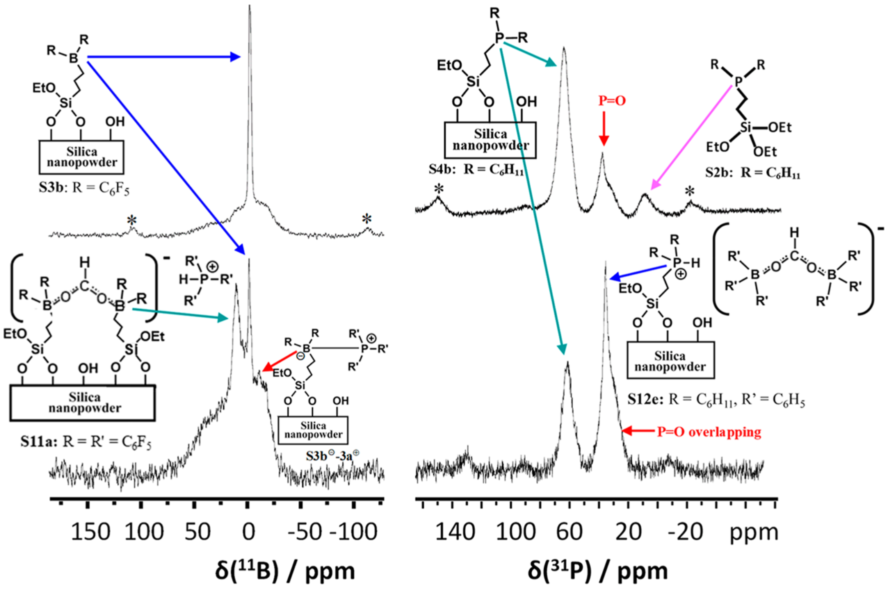

**Figure 9.** (left) $^{11}$B CP MAS NMR spectra of **S3b** and **S11a** (the supported diborano formate that was purposefully prepared by the reaction between externally added HCOOH and **S3b/3a**). (right) $^{31}$P CP MAS NMR spectra of **S4b** (top) and **S12e** (bottom). The resonances of the oxidized side products of **S4b** and **S12e** are labeled P═O in red. The resonance of **S2b** on the $^{31}$P CP MAS NMR spectrum of **S4b** is also labeled as this a remnant of the reactant that was used to synthesize **S4b** (see Scheme 1). Spinning sidebands are labeled with asterisks.

$C_6H_5$ substituents on the boranes and phosphines gave more effective $CO_2$ capture and conversion to HCOOH in comparison to electron-poor $C_6F_5$ or electron-donating $C_6H_{11}$ substituents. ATR FTIR combined with solid-state $^{13}$C NMR spectroscopy was found to be a very useful technique to qualitatively compare the conversion success of different FLP systems. Five out of the 12 silica nanopowder supported FLP systems also reacted with the newly generated HCOOH to form limited amounts of a diborano formate species. It is concluded that the immobility of silica nanopowder bound Lewis acids (or Lewis bases) is the main reason HCOOH actually can be liberated rather than killing the FLP capability to generate HCOOH by diborano formate formation. The use of $^{11}$B and $^{31}$P CP MAS NMR further demonstrated that when the immobilized FLP becomes too sterically hindered, as is the case with Mes-containing FLP systems, HCOOH formation and $CO_2$ capture fail. However, when the sterically hindered environment of the FLPs is relieved too much, then the advantage of using nanopowder silica carriers is annihilated because normal Lewis acid−base adducts begins to form. It is concluded that an optimum hindrance configuration exists for each application of FLPs, here to capture $CO_2$ and reduce it to HCOOH. Research is at present focused on developing and determining FLP system lifetimes, conversion numbers, and shelf lives of these unique new heterogeneously supported FLP systems in $CO_2$ conversion to HCOOH.

## ■ ASSOCIATED CONTENT

### Supporting Information

The Supporting Information is available free of charge at https://pubs.acs.org/doi/10.1021/acs.inorgchem.0c02012.

$^1$H NMR, XPS, and ATR FTIR spectra (PDF)

## ■ AUTHOR INFORMATION

### Corresponding Author

**Elizabeth Erasmus** − *Department of Chemistry, University of the Free State, Bloemfontein 9300, South Africa;* orcid.org/0000-0003-0546-697X; Phone: ++27-51-4019656; Email: ErasmusE@ufs.ac.za; Fax: ++27-51-4017295

### Authors

**Kgauhelo Mentoor** − *Department of Chemistry, University of the Free State, Bloemfontein 9300, South Africa*
**Linette Twigge** − *Department of Chemistry, University of the Free State, Bloemfontein 9300, South Africa*
**J. W. Hans Niemantsverdriet** − *SynCat@DIFFER, Syngaschem BV, 5612 AJ Eindhoven, The Netherlands*
**Jannie C. Swarts** − *Department of Chemistry, University of the Free State, Bloemfontein 9300, South Africa;* orcid.org/0000-0003-2608-0371

Complete contact information is available at: https://pubs.acs.org/10.1021/acs.inorgchem.0c02012

### Notes

The authors declare no competing financial interest.

## ■ ACKNOWLEDGMENTS

This work has received support from the University of the Free State (K.M., L.T., J.C.S. and E.E.), South African National Research Foundation Grants 119028 (E.E.) and 96123 (J.C.S.) and the Central Research Fund of the University of the Free State, Bloemfontein, South Africa. Funding is also acknowledged from Synfuels China Technology Co. Ltd., Beijing-Huairou, People's Republic of China (J.W.N.), and Syngaschem BV, The Netherlands (J.C.S. and E.E.).

## ■ REFERENCES

(1) Federsel, C.; Jackstell, R.; Beller, M. State-of-the-Art Catalysts for Hydrogenation of Carbon Dioxide. *Angew. Chem., Int. Ed.* **2010**, *49* (36), 6254−6257.

(2) Liu, Q.; Wu, L.; Jackstell, R.; Beller, M. Using Carbon Dioxide as a Building Block in Organic Synthesis. *Nature Communications* **2015**, *6*, 5933.

(3) McCahill, J. S. J.; Welch, G. C.; Stephan, D. W. Reactivity of "Frustrated Lewis Pairs": Three-Component Reactions of Phosphines,

a Borane, and Olefins. *Angew. Chem., Int. Ed.* **2007**, *46* (26), 4968−4971.

(4) Welch, G. C.; Cabrera, L.; Chase, P. A.; Hollink, E.; Masuda, J. D.; Wei, P.; Stephan, D. W. Tuning Lewis Acidity Using the Reactivity of "Frustrated Lewis Pairs": Facile Formation of Phosphine-Boranes and Cationic Phosphonium-Boranes. *J. Chem. Soc. Dalt. Trans.* **2007**, No. 31, 3407−3414.

(5) Courtemanche, M.-A.; Légaré, M.-A.; Maron, L.; Fontaine, F.-G. A Highly Active Phosphine-Borane Organocatalyst for the Reduction of $CO_2$ to Methanol Using Hydroboranes. *J. Am. Chem. Soc.* **2013**, *135* (25), 9326−9329.

(6) Lim, C. H.; Holder, A. M.; Hynes, J. T.; Musgrave, C. B. Reduction of $CO_2$ to Methanol Catalyzed by a Biomimetic Organo-Hydride Produced from Pyridine. *J. Am. Chem. Soc.* **2014**, *136* (45), 16081−16095.

(7) Menard, G.; Stephan, D. W. Room Temperature Reduction of CO $_2$ to Methanol by Al-Based Frustrated Lewis Pairs and Ammonia Borane. *J. Am. Chem. Soc.* **2010**, *132* (6), 1796−1797.

(8) Sgro, M. J.; Stephan, D. W. Activation of $CO_2$ by Phosphinoamide Hafnium Complexes. *Chem. Commun.* **2013**, *49* (26), 2610−2612.

(9) Stephan, D. W.; Erker, G. Frustrated Lewis Pairs: Metal-Free Hydrogen Activation and More. *Angew. Chem., Int. Ed.* **2010**, *49* (1), 46−76.

(10) Jupp, A. R.; Stephan, D. W. New Directions for Frustrated Lewis Pair Chemistry. *Trends Chem.* **2019**, *1* (1), 35−48.

(11) Stephan, D. W. The Broadening Reach of Frustrated Lewis Pair Chemistry. *Science* **2016**, *354*, aaf7229.

(12) Stephan, D. W. Frustrated Lewis Pairs: From Concept to Catalysis. *Acc. Chem. Res.* **2015**, *48* (2), 306−316.

(13) Stephan, D. W.; Erker, G. Frustrated Lewis Pairs: Metal-Free Hydrogen Activation and More. *Angew. Chem., Int. Ed.* **2010**, *49*, 46−76.

(14) Song, Q. W.; Zhou, Z. H.; He, L. N. Efficient, Selective and Sustainable Catalysis of Carbon Dioxide. *Green Chem.* **2017**, *19*, 3707−3728.

(15) Lu, G.; Zhang, P.; Sun, D.; Wang, L.; Zhou, K.; Wang, Z.-X.; Guo, G.-C. Gold Catalyzed Hydrogenations of Small Imines and Nitriles: Enhanced Reactivity of Au Surface toward $H_2$ via Collaboration with a Lewis Base. *Chem. Sci.* **2014**, *5* (3), 1082−1090.

(16) Trunk, M.; Teichert, J. F.; Thomas, A. Room-Temperature Activation of Hydrogen by Semi-Immobilized Frustrated Lewis Pairs in Microporous Polymer Networks. *J. Am. Chem. Soc.* **2017**, *139* (10), 3615−3618.

(17) Willms, A.; Schumacher, H.; Tabassum, T.; Qi, L.; Scott, S. L.; Hausoul, P. J. C.; Rose, M. Solid Molecular Frustrated Lewis Pairs in a Polyamine Organic Framework for the Catalytic Metal-Free Hydrogenation of Alkenes. *ChemCatChem* **2018**, *10* (8), 1835−1843.

(18) Mahdi, T.; Stephan, D. W. Facile Protocol for Catalytic Frustrated Lewis Pair Hydrogenation and Reductive Deoxygenation of Ketones and Aldehydes. *Angew. Chem., Int. Ed.* **2015**, *54* (29), 8511−8514.

(19) Xing, J. Y.; Buffet, J. C.; Rees, N. H.; Nørby, P.; O'Hare, D. Hydrogen Cleavage by Solid-Phase Frustrated Lewis Pairs. *Chem. Commun.* **2016**, *52* (69), 10478−10481.

(20) Wanglee, Y.-J.; Hu, J.; White, R. E.; Lee, M.-Y.; Stewart, S. M.; Perrotin, P.; Scott, S. L. Borane-Induced Dehydration of Silica and the Ensuing Water-Catalyzed Grafting of $B(C_6F_5)_3$ To Give a Supported, Single-Site Lewis Acid, $\equiv SiOB(C_6F_5)_2$. *J. Am. Chem. Soc.* **2012**, *134* (1), 355−366.

(21) Szeto, K. C.; Sahyoun, W.; Merle, N.; Castelbou, J. L.; Popoff, N.; Lefebvre, F.; Raynaud, J.; Godard, C.; Claver, C.; Delevoye, L.; Gauvin, R. M.; Taoufik, M. Development of Silica-Supported Frustrated Lewis Pairs: Highly Active Transition Metal-Free Catalysts for the Z-Selective Reduction of Alkynes. *Catal. Sci. Technol.* **2016**, *6* (3), 882−889.

(22) Zakharova, M. V.; Masoumifard, N.; Hu, Y.; Han, J.; Kleitz, F.; Fontaine, F. G. Designed Synthesis of Mesoporous Solid-Supported Lewis Acid-Base Pairs and Their $CO_2$ Adsorption Behaviors. *ACS Appl. Mater. Interfaces* **2018**, *10* (15), 13199−13210.

(23) Erasmus, E. X-Ray Photoelectron Spectroscopy: Charge Transfer in Fe 2p Peaks and Inner-Sphere Reorganization of Ferrocenyl-Containing Chalcones. *J. Electron Spectrosc. Relat. Phenom.* **2018**, *223*, 84.

(24) Gerber, S. J.; Erasmus, E. Electronic Effects of Metal Hexacyanoferrates: An XPS and FTIR Study. *Mater. Chem. Phys.* **2018**, *203*, 73.

(25) Erasmus, E. Electronic Effects of Group Fragments on the XPS of Fe 2p and 3p Photoelectron Lines of Ferrocenyl-Containing Chalcones. *S. Afr. J. Chem.* **2017**, *70*, 70.

(26) Gostynski, R.; Conradie, J.; Erasmus, E. Significance of the Electron-Density of Molecular Fragments on the Properties of Manganese(III) *β*-Diketonato Complexes: An XPS and DFT Study. *RSC Adv.* **2017**, *7* (44), 27718−27728.

(27) Buitendach, B. E.; Erasmus, E.; Landman, M.; Niemantsverdriet, J. W. H.; Swarts, J. C. Consequences of Electron-Density Manipulations on the X-Ray Photoelectron Spectroscopic Properties of Ferrocenyl-*β*-Diketonato Complexes of Manganese(III). Structure of [Mn-$(FcCOCHCOCH_3)_3$]. *Inorg. Chem.* **2016**, *55* (5), 1992.

(28) Buitendach, B. E.; Erasmus, E.; Niemantsverdriet, J. W.; Swarts, J. C. Properties of Manganese(III) Ferrocenyl-*β*-Diketonato Complexes Revealed by Charge Transfer and Multiplet Splitting in the Mn 2p and Fe 2p X-Ray Photoelectron Envelopes. *Molecules* **2016**, *21* (11), 1427.

(29) Erasmus, E.; Niemantsverdriet, J. W.; Swarts, J. C. Preparation and Characterization of Supported Bimetallic $Pd^{IV}$-$Co^{III}$ Model Catalyst from Organometallic Single Source Precursor for Aerobic Oxidation of Alcohols. *Langmuir* **2012**, *28* (47), 16477.

(30) Parks, D. J.; Rupert, R. E.; Piers, W. E. Bis(Pentafluorophenyl)-Borane: Synthesis, Properties, and Hydroboration Chemistry of a Highly Electrophilic Borane Reagent. *Angew. Chem., Int. Ed. Engl.* **1995**, *34* (7), 809−811.

(31) Britovsek, G. J. P.; Ugolotti, J.; White, A. J. P. From $B(C_6F_5)_3$ to $B(OC_6F_5)_3$: Synthesis of $(C_6F_5)_2BOC_6F_5$ and $C_6F_5B(OC_6F_5)_2$ and Their Relative Lewis Acidity. *Organometallics* **2005**, *24* (7), 1685−1691.

(32) Moulder, J. F.; Stickle, W. F.; Sobol, P. E.; Bomben, K. D. *Handbook of X-Ray Photoelectron Spectroscopy*; Perkin-Elmer: Eden Prairie, MN, 1992, 2002.

(33) Batan, A.; Franquet, A.; Vereecken, J.; Reniers, F. Characterisation of the Silicon Nitride Thin Films Deposited by Plasma Magnetron. *Surf. Interface Anal.* **2008**, *40* (3−4), 754−757.

(34) Liu, T.; Ma, X.; Liu, D.; Hao, S.; Du, G.; Ma, Y.; Asiri, A. M.; Sun, X.; Chen, L. Mn Doping of CoP Nanosheets Array: An Efficient Electrocatalyst for Hydrogen Evolution Reaction with Enhanced Activity at All PH Values. *ACS Catal.* **2017**, *7* (1), 98−102.

(35) Conradie, M. M.; Conradie, J.; Erasmus, E. Immobilisation of Iron Tris(*β*-Diketonates) on a Two-Dimensional Flat Amine Functionalised Silicon Wafer: A Catalytic Study of the Formation of Urethane, from Ethanol and a Diisocyanate Derivative. *Polyhedron* **2014**, 52−59.

(36) Conradie, J.; Erasmus, E. XPS Fe 2p Peaks from Iron Tris(*β*-Diketonates): Electronic Effect of the *β*-Diketonato Ligand. *Polyhedron* **2016**, 142−150.

(37) Zhao, X.; Stephan, D. W. Bis-Boranes in the Frustrated Lewis Pair Activation of Carbon Dioxide. *Chem. Commun.* **2011**, *47* (6), 1833.

(38) Stephan, D. W.; Erker, G. Frustrated Lewis Pair Chemistry of Carbon, Nitrogen and Sulfur Oxides. *Chem. Sci.* **2014**, *5* (7), 2625−2641.

(39) Tolman, C. A. Steric Effects of Phosphorus Ligands in Organometallic Chemistry and Homogeneous Catalysis. *Chem. Rev.* **1977**, *77* (3), 313−348.

(40) Tolman, C. A. Phosphorus Ligand Exchange Equilibriums on Zerovalent Nickel. Dominant Role for Steric Effects. *J. Am. Chem. Soc.* **1970**, *92* (10), 2956−2965.

(41) Ashley, A. E.; O'Hare, D. FLP-Mediated Activations and Reductions of $CO_2$ and CO. *Top. Curr. Chem.* **2012**, *334*, 191−217.

(42) Ye, J.; Johnson, J. K. Screening Lewis Pair Moieties for Catalytic Hydrogenation of $CO_2$ in Functionalized UiO-66. *ACS Catal.* **2015**, *5* (10), 6219−6229.

(43) Ye, J.; Johnson, J. K. Catalytic Hydrogenation of $CO_2$ to Methanol in a Lewis Pair Functionalized MOF. *Catal. Sci. Technol.* **2016**, *6* (24), 8392−8405.

(44) Ye, J.; Johnson, J. K. Design of Lewis Pair-Functionalized Metal Organic Frameworks for $CO_2$ Hydrogenation. *ACS Catal.* **2015**, *5* (5), 2921−2928.

(45) Peuser, I.; Neu, R. C.; Zhao, X.; Ulrich, M.; Schirmer, B.; Tannert, J. A.; Kehr, G.; Fröhlich, R.; Grimme, S.; Erker, G.; Stephan, D. W. $CO_2$ and Formate Complexes of Phosphine/Borane Frustrated Lewis Pairs. *Chem. - Eur. J.* **2011**, *17* (35), 9640−9650.

(46) Bergantini, A.; Pilling, S.; Rothard, H.; Boduch, P.; Andrade, D. P. P. Processing of Formic Acid-Containing Ice by Heavy and Energetic Cosmic Ray Analogues. *Mon. Not. R. Astron. Soc.* **2014**, *437* (3), 2720−2727.

(47) Khanna, R. K.; Lowenthal, M. S.; Ammon, H. L.; Moore, M. H. Molecular Structure and Infrared Spectrum of Solid Amino Formate ($HCO_2NH_2$): Relevance to Interstellar Ices. *Astrophys. J., Suppl. Ser.* **2002**, *140* (2), 457−464.

(48) Erasmus, E.; Claassen, J.; Van der Westhuizen, W. Catalytic Wet Peroxide Oxidation of Formic Acid in Wastewater with Naturally-Occurring Iron Ore. *Water SA* **2016**, *42* (3), 442.

(49) Cabilla, G. Infrared Study of the Adsorption of Formic Acid on Clean and Ca-Promoted Pd/$SiO_2$ Catalysts. *Appl. Catal., A* **2003**, *255* (2), 181−195.

(50) Popova, G. Y.; Andrushkevich, T. V.; Chesalov, Y. A.; Stoyanovv, E. S. In situ FTIR Study of the Adsorption of Formaldehyde, Formic Acid, and Methyl Formiate at the Surface of $TiO_2$(Anatase). *Kinetics and Catalysis* **2000**, *41*, 805−811.

(51) Millar, G. J.; Rochester, C. H.; Waugh, K. C. An FTIR Study of the Adsorption of Formic Acid and Formaldehyde on Potassium-Promoted Cu/$SiO_2$ Catalysts. *J. Catal.* **1995**, *155* (1), 52−58.

(52) Liu, L.; Vankovaa, N.; Heinea, T. A Kinetic Study on the Reduction of $CO_2$ by Frustrated Lewis Pairs: From Understanding to Rational Design. *Phys. Chem. Chem. Phys.* **2016**, *18* (5), 3567−3574.

(53) Wiegand, T.; Siedow, M.; Eckert, H.; Kehr, G.; Erker, G. Structural Characterization of Frustrated Lewis Pairs and Their Reaction Products Using Modern Solid-State NMR Spectroscopy Techniques. *Isr. J. Chem.* **2015**, *55*, 150−178.

(54) Hunter, A. D.; Williams, T. R.; Zarzyczny, B. M.; Bottesch, H. W. I.; Dolan, S. A.; McDowell, K. A.; Thomas, D. N.; Mahler, C. N. Correlations among $^{31}$P NMR Coordination Chemical Shifts, Ru-P Bond Distances, and Enthalpies of Reaction in $Cp'Ru(PR_3)_2Cl$ Complexes ($Cp'$ = ;$_5$-$C_5H_5$, ;$_5$-$C_5Me_5$; $PR_3$ = $PMe_3$, $PPhMe_2$, $PPh_2Me$, $PPh_3$, $PEt_3$, $PnBu_3$). *Organometallics* **2016**, *35* (16), 2701−2706.

(55) Clark, H. C. S.; Coleman, K. S.; Fawcett, J.; Holloway, J. H.; Hope, E. G.; Langer, J.; Smith, I. M. Reactions of Iridium and Rhodium Hydrides with Anhydrous HF; Crystal Structure of $[Rh(CO)(PPh_3)_3]$-$[BF_4]$·Thf. *J. Fluorine Chem.* **1998**, *91* (2), 207−211.